Journal of Geography and Geology; Vol. 10, No. 3; 2018
ISSN 1916-9779 E-ISSN 1916-9787
Published by Canadian Center of Science and Education

Interconnected Accommodation Space Controls Between Sand-Charged Shallow Tidal Channels and Wind-Wave Truncated Tidal Flats During Latest-Holocene Sea Level Rise (~3.0 m) in a Large Mesotidal Wave-Dominated Estuary, Grays Harbor, Washington, USA

Curt D. Peterson[1] & Sandy Vanderburgh[2]

[1] Geology Department, Portland State University, Portland, United States

[2] Medicine Hat College, Medicine Hat, Canada

Correspondence: Curt Peterson, Geology Department, Portland State University, Portland, OR., 97207, United States. Tel: 1-503-730-9266. E-mail: curt.d.peterson@gmail.com

Received: July 15, 2018 Accepted: July 27, 2018 Online Published: August 12, 2018

doi:10.5539/jgg.v10n3p26 URL: http://dx.doi.org/10.5539/jgg.v10n3p26

The research is financed by the United States Geological Survey and Medicine Hat College, Alberta, Canada

Abstract

The late-Holocene (5–0 ka) record of accommodation space controls of tidal channel and tidal flat deposition in the shallow mesotidal wave-dominated Grays Harbor estuary (236 km^2 surface area) was investigated in previously reported drill cores (n=15) and new vibracores (n=20), reaching 3–10 m depth subsurface. Continuous vibracore facies sequences (3–4 m depth subsurface) discriminate between tidal channel and tidal flat deposition and demonstrate responses of both depositional settings to interseismic uplift and coseismic subsidence (1±0.5 m vertical) from cyclic neotectonic forcing (200–800 yr recurrence intervals) in the Cascadia subduction zone. Vibracore channel samples, at 0.5 m or 1.0 m depth intervals, were analyzed for sediment grain size (sample n=124) and sand source mineralogy (sample n=67). The mean and standard deviation of sand size in the sand fraction is 175±x34 1σ μm. Sediment ^{14}C dates (n=29) range from 376 to 6,579 median calyrBP and establish long-term sedimentation rates in subtidal channel accretionary banks (average 4.2 m ka^{-1}), intertidal channel accretionary banks (average 3.7 m ka^{-1}), and tidal flats (average 1.1 m ka^{-1}). Tidal channel accretionary bank deposition largely reflects reworking of pre-existing estuary deposits. Long-term total basin sediment accumulation rates ($232x10^6$ m^3 ka^{-1}) are tied to rates of net sea level rise (1.0 m ka^{-1}) or increasing basin accommodation space. In latest Holocene time (3–0 ka) littoral sand import ($117x10^6$ m3 ka^{-1}) was about twice as large as the retention of river sand and mud in the estuary. The selective export of winnowed mud from the estuary provided the necessary accommodation space for the import of littoral sand in latest-Holocene time. Shallow intertidal settings in Grays Harbor (60% by surface area) are maintained by self-regulating conditions of channelized sediment import, wind-wave erosion of tidal flats, and tidal prism forcing of tidal channel discharge. Hind-casted wind-wave bottom orbital velocities (>20 cm sec^{-1}) are sufficient to truncate tidal flat elevations to lower-intertidal levels, which maintain substantial tidal prism volumes (modern MLLW-MHHW ~6.1×10^8 m^3) and associated tidal channel discharge in the shallow estuary. Net sediment deposition in the estuary is controlled by the interaction of limiting accommodation space controls in the tidal flats and tidal channels. The balance between sediment supply, energy of sediment transport/resuspension, and sediment export has survived small changes in relative sea level (1±0.5 m) from cyclic neotectonic forcing. However, the prehistoric (natural) balance could be altered by future anthropogenic impacts from sustained global sea level rise (> 1.5 m during the next century) or diminished wind-wave fetch distances, which could result from tidal flat diking/filling or uncontrolled spread of non-native invasive stabilizing sea grass (*Spartina*). In this regard, the susceptibilities of prehistorically-balanced sediment dynamics in Grays Harbor serve as warning for other similar mesotidal wave-dominated estuaries that could be impacted by future global sea level rise, changing sediment inputs, and/or tidal flat diking/filling, which could reduce intertidal habitat and associated ecosystem functions.

Keywords: tidal flat, tidal channel, deposition, mesotidal estuary, late Holocene, marine transgression, wind waves

1. Introduction

How might accommodation space limitations in comingled tidal channels and lower-intertidal flats have interacted to control depositional processes in shallow wave-dominated estuaries during the late-Holocene marine transgression? Grays Harbor (~236 km^2 in size) has ideal geomorphic, hydrographic, and sediment supply conditions to investigate such accommodation space limitations (Peterson & Phipps, 2016). These conditions occur, in part, due to the location of Grays Harbor within the high-energy and sand-rich Columbia River Littoral Cell (CRLC) system (Figure 1). Unlike the nearby fluvial-tidal Columbia River estuary that is highly channelized (Peterson et al., 2014) and the tidally-dominated hydrography of Willapa Bay, with its broad marginal shallow tidal flats (Clifton & Phillips, 1980; Peterson & Vanderburgh, 2018), the Grays Harbor estuary demonstrates a close intermingling of both depositional settings. Like those other two large estuaries in the CRLC system, Grays Harbor has experienced episodic coseismic subsidence events (1±0.5 m paleo-tidal level change at 300–800 yr recurrence intervals) from megathrust ruptures in the Cascadia subduction zone (Atwater, 1997; Atwater et al, 2004). Such neotectonic cycles of interseismic uplift and coseismic subsidence had a negligible impact on fluvial-tidal deposition in the Columbia River estuary (Peterson et al., 2014), but substantial impacts on marginal tidal flat deposition in Willapa Bay (Peterson & Vanderburgh, 2018). The potential influence of such neotectonic cycles of sea level change on depositional processes in tidal channels and lower-intertidal flats in Grays Harbor have not previously been investigated. Another common factor between all three estuaries is seasonally-strong onshore wind flow (Byrnes & Li, 1998), which yields energetic wind-waves in the large shallow estuaries of the CRLC system. Such locally-generated wind-waves have had important roles in limiting upper-intertidal accommodation space in both the Columbia River estuary (Peterson et al., 2014) and Willapa Bay (Peterson & Vanderburgh, 2018), but that case has yet to be made for the intermingled tidal channels and tidal flats in Grays Harbor.

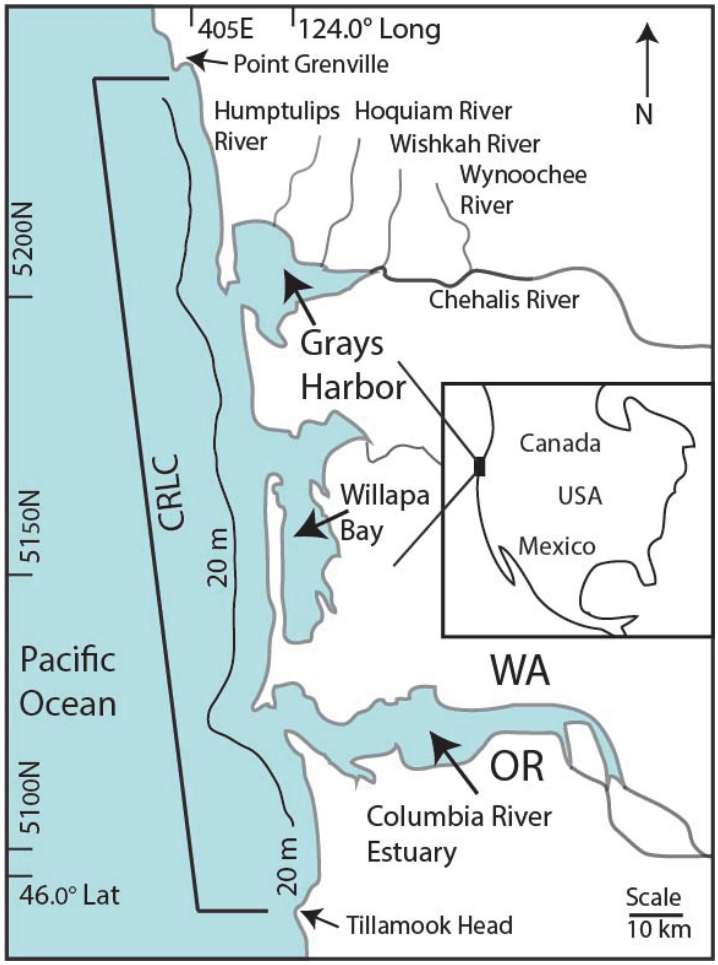

Figure 1. Map of Grays Harbor and adjacent large estuaries in the study region

Grays Harbor, Willapa Bay and the Columbia River Estuary occur within the Columbia River Littoral Cell (CRLC) system, extending from Tillamook Head in Northwest Oregon to Point Grenville in Southwest Washington

(alongshore distance ~ 160 km). Columbia River sand that bypasses the Columbia River estuary feeds the inner-shelf, adjacent beaches, Willapa Bay, and Grays Harbor with abundant fine sand.

Depositional accommodation space has been applied both as a quantified basing filling parameter for submerged incised valleys (Peterson & Scheidegger, 1984; Peterson & Phipps, 1992) and as a conceptual model for incised valley deposition during transgressive submergence (Allen & Posamentier, 1993; Dalrymple et al., 1994; Zaitlin et al., 1994). Accommodation space relations helped to establish net sediment transport directions and sediment partitioning in the complex CRLC system throughout the Holocene period. The Columbia River bypassed sand through its estuary to the littoral zone during the Holocene marine transgression (Baker et al., 2010). A net-northward transport in the inner-shelf (Twichell et al., 2010; Peterson et al., 2016) supplied littoral sand to the Grays Harbor estuary, near the northern end of the CRLC system, by ~12 ka (Peterson & Phipps, 2016). The Grays Harbor estuary evolved into its present configuration of shallow tidal flats protected from the high-wave energy littoral zone (Ruggiero et al., 1997) behind the north and south sand spits by late-Holocene time (~5 ka) (Vanderburgh et al., 2010). The tidal inlet has remained largely in place as the Grays Harbor sand spits prograded seaward (~2.0 km) during latest-Holocene time.

In this study, accommodation space controls are investigated in tidal channels and tidal flats of Grays Harbor using 1) tidal flat elevations, 2) deposit facies sequences (2–4 m depth), 3) latest-Holocene sedimentation rates, and 4) bottom orbital velocity estimates from modern wind wave forcing. In this article, we transition from previous studies of longer-term depositional records (12–0 ka) in the Grays Harbor estuary (Peterson & Phipps, 1992; Phipps et al., 2015; Peterson & Phipps, 2016) to the latest-Holocene period (3–0 ka) of decreased rates of net sea level rise. This transition to the latest-Holocene interval of basin filling in Grays Harbor helps to establish the potential roles of shallow tidal channels and lower-intertidal flats in controlling basin sediment accumulation rates under condition of several meters of net sea level rise. In this regard, Grays Harbor serves as an exceptional analog for other shallow mesotidal estuaries that could experience near future sea level rise from ongoing global warming (Kopp et al., 2014). The shallow lower-intertidal settings in Grays Harbor are shown to be buffered with respect to small changes in sediment supply and sea level. However, these settings could be susceptible to 1) progressive submergence from future global sea level rise, 2) shoaling of the shallow tidal flats from diking and filling, and/or 3) shoaling of interior tidal flats from an uncontrolled spread of invasive non-native stabilizing vegetation *Spartina* (WSDA, 2016).

2. Background

The hydrographic ratio (H_r=tidal prism discharge/6-hr mean river discharge) of the Grays Harbor estuary (H_r=86:1) is intermediate between that of the nearby fluvial-tidal Columbia River estuary (H_r=5:1) (Figure 1) and the nearly fully-tidal hydrography of Willapa Bay (H_r=232) (Peterson et al., 1984). All three estuaries are co-located in the CRLC system, which has been abundantly supplied by fine sand during the middle- ad late-Holocene marine transgression from the large Columbia River (Peterson et al., 2010; Baker et al., 2010; Peterson et al., 2016). The three estuaries are exposed to strong-onshore winds (Byrnes & Li, 1998), which are superimposed on mixed semi-diurnal mesotidal ranges (~3 m). These conditions have led to relatively shallow estuarine bathymetries, but not to floodplain or tidal marsh infilling of the lower- to middle-estuarine reaches. Grays Harbor estuary is characterized by an intermingling of shallow (< 10 m depth) dendritic tidal channels and dissected lower-intertidal flats (Figure 2). These co-existing environments in Grays Harbor provide an opportunity to examine the transport and depositional responses of both shallow tidal channels and lower-intertidal flats to abundant sediment supply, changing sea levels, and energetic current flows in a large shallow wave-dominated estuary.

The modern hydrographic and/or geomorphic areas of Grays Harbor have been divided into five sub-regions by Milliman (1963), including 1) the Channel Entrance or tidal inlet, 2) the Outer Harbor, impacted by diminishing ocean wave energy with increasing distance inshore from the tidal inlet, 3) the North Bay, protected behind the north spit, 4) the South Bay, as divided into northern tidal flats and southern tidal marsh, on either side of the HW105 Bridge, and 5) the Inner Harbor, with decreasing wind-wave exposure with increasing distance up (eastward) the narrowing river valley (Figure 2, Table 1). The Grays Harbor surface area, from the HW101 bridge to the Harbor mouth jetties, totals 232 km^2, as converted from Milliman (1963) by Barrick (1976). An independent planimetric analysis of the estuary total surface area based on the USC&GS nautical chart 6195 (USCGS, 1973) yielded a 4% difference (less than) the Milliman total surface area (Barrick, 1976). The Chehalis River channel is constricted by prograded upper-intertidal to supratidal floodplains, > 1.5 m mean tidal level (MTL), upstream of the HW101 bridge (Figure 2). Wave swept sand shoals along channel banks of the outer harbor might include remobilized dredge spoils from maintenance deepening of the shipping channel, 10–15 m channel water depth. About 60 percent of the estuary's surface area is exposed at lowest tide (Barrick, 1976). Mean higher high water (MHHW) in Grays Harbor is taken to be 2.7 m above mean lower low water (MLLW), with maximum tidal ranges

reaching ~3.0 m. Grays Harbor lacks a deep central basin, but it also lacks substantial tidal marsh or flood plain progadation seaward of the HW101 bridge in the constricted upper estuarine reaches. The central estuarine reaches vertically accreted to shallow intertidal depths by late-Holocene time (Peterson & Phipps, 2016). But unlike the floodplain constricted uppermost reaches of the tidally influenced tributary valleys, the central and lower reaches of Grays Harbor ceased to fill-in to upper-intertidal salt marsh or supratidal flood plain elevations. Modern sediments in Grays Harbor were investigated for grain size distributions and heavy-mineral indicators of river versus littoral sand sources (Phipps et al., 1976; Scheidegger & Phipps, 1976). Dominant sand supplies transition from littoral sources in the Outer Harbor sub-region to river sources in the Inner Harbor sub-region and the northernmost North Bay sub-region. Jetty construction, diking, dredging and dredge spoils disposal in Grays Harbor during historic time (early 1900s to present) could have influenced the compositions of the modern deposits examined by Scheidegger & Phipps (1976). The dated vibracores obtained in this study extend to latest-prehistoric time, so they include sections that were not influenced by industrial anthropogenic activities.

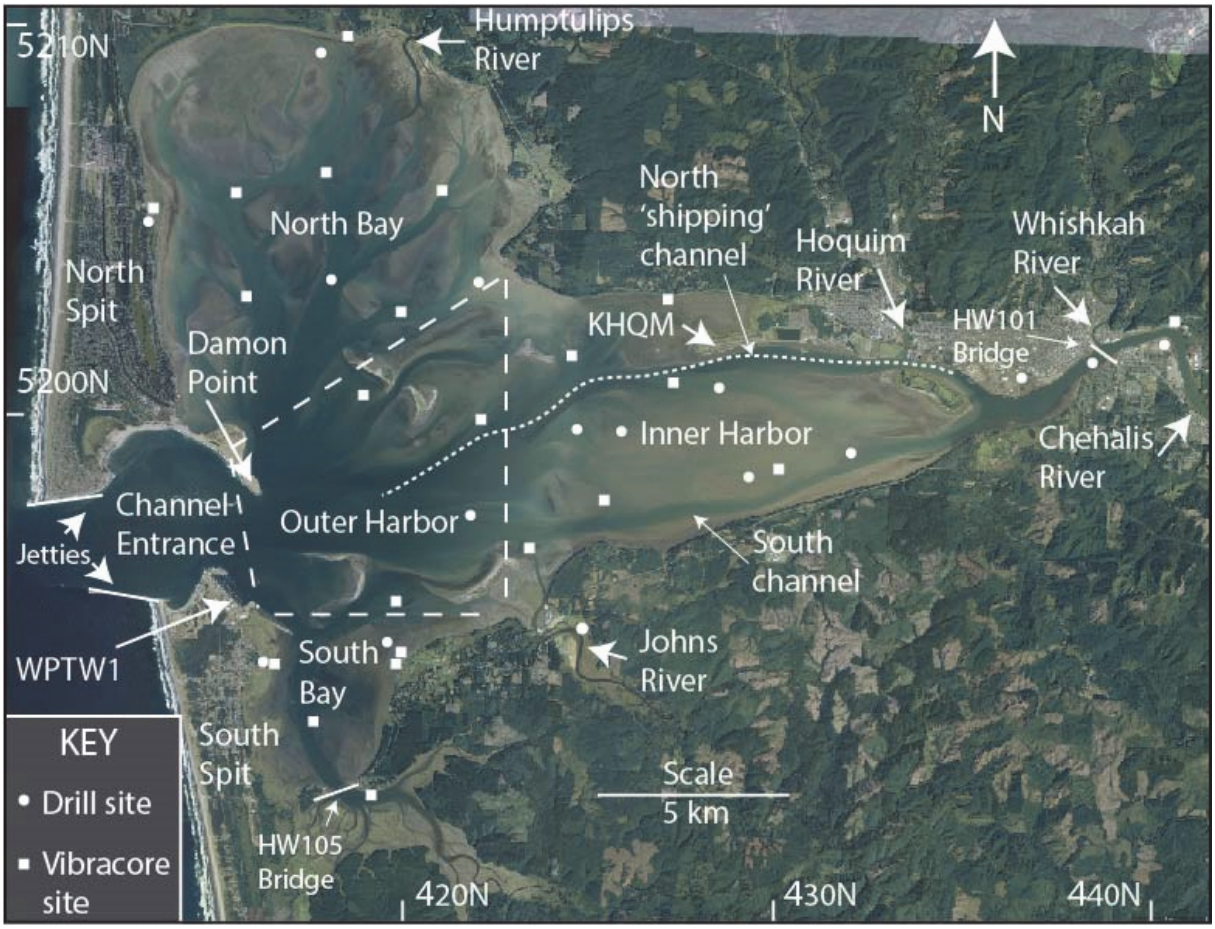

Figure 2. Map of modern physiography and core sites in Grays Harbor estuary

Details about previously reported drill sites (solid squares) and newly reported vibracore sites (solid circles), including site numbers, position coordinates, and site elevations are presented below. Satellite images, that were recorded during a spring low tide, June 2009, are from Google Earth (2018). Sub-regions (dashed lines) in the estuary are redrawn from Milliman (1963).

Table 1. Modern harbor, tidal surface areas and bathymetric volumes in Grays Harbor

Sub-regions	Area (km^2)
Channel Entrance	16
Outer Harbor	46

North Bay	87
Northern South Bay	15
Southern South Bay	8
Inner Harbor	60
Total	232

Tidal level	Area (km^2)	Volume ($x10^8 m^3$)
MLLW	98	3.9
MLW	119	4.3
Mean	171	6.4
MHW	223	9.4
MHHW	233	10.0
Maximum HW	236	10.5

Notes: Sub-region surface areas are taken from the HW101 Bridge to the seaward extents of the Channel Entrance jetties (Milliman, 1963), as shown in Figure 2. Tidal surface areas and volumes are taken from the Whynoche River confluence with the Chehalis River (Figure 1) to the seaward extent of the Channel Entrance jetties and to the HW105 bridge in South Bay (Stein et al., 1966), based on the United States Coast and Geodetic Survey Bathymetric Chart 6195 (USCGS, 1973). All surface area data are converted from statue miles and cubic yards as summarized by Knotts & Barrick (1976), to square kilometers and cubic meters (this article).

The long-term depositional response of the Grays Harbor estuary to changing rates of sea level rise during the Holocene marine transgression was investigated with seismic reflection profiling, drill core sampling, and radiocarbon dating of recovered drill core sections (Figure 2) (Peterson & Phipps,1992). Analyses of river and littoral sediment in-flux into the Grays Harbor estuary were compared to sea level and sediment level curves to establish basin-wide accommodation space controls on depositional sequences and littoral sediment sinks in the submerged incised valley (Peterson & Phipps, 2016). One transitional event proved to be particularly important in the depositional evolution of the Grays Harbor estuary. The mid-Holocene filling of the central basin in Grays Harbor by river sand and mud eliminated a deeper central basin bathymetry by late-Holocene time (Peterson & Phipps, 2016). The presence of such a deep basin (Dalyrymple, 1992) could have restricted the inshore transport of littoral sand to the interior reaches of the estuary. The central basin filling in Grays Harbor lead to constricted shallow tidal channels and lower-intertidal tidal flats throughout the lower and middle reaches of the evolving estuary. These constricted and/or shallow-water settings apparently facilitated an ongoing in-flux of littoral sand and out-flux (bypassing) of river mud though the lower estuarine reaches to the offshore littoral zone. However, the potential mechanisms of sediment transport and deposition in the shallow tidal channels and tidal flat settings in Grays Harbor that permitted the coeval in-flux of littoral sand and out-flux of fluvial sediments were not established by Peterson & Phipps (1992). Nor were the mechanism(s) by which the estuary maintained its dendritic network of shallow sandy tidal channels and intervening muddy sand tidal flats under conditions of abundant river mud supply (Peterson & Phipps, 2016). This article now addresses such potential mechanisms under generalized models of accommodation space controls in the large shallow mesotidal wave-dominated estuary.

3. Methods

Rotary drill core sites (D), as shown in Figure 3 and Table 2, were positioned in subtidal channels or submerged tidal flats located adjacent to intertidal channels (Peterson & Phipps, 1992). Drilling was conducted from a side-mounted platform on a four-point anchored drilling barge. Exceptions are D2 and D4, which were drilled on gravel-fill ramps constructed over narrow salt marsh shorelines. Sites A1–4 were sampled by hollow-stem auger drilling through artificial fill over a tidal marsh/floodplain (Phipps et al., 2015). Drill core sites were sampled by hydraulic ram coring (50 cm long cores) at either 1.5 or 3.0 m depth intervals downhole for sediment source, texture, and radiocarbon sample dating (Peterson & Phipps, 2016). Continuous shallow vibracores (2–4 m depth subsurface) were obtained to compliment the drill core sampling with high-resolution depositional records from lower-intertidal channel banks and lower-intertidal flats, as described below.

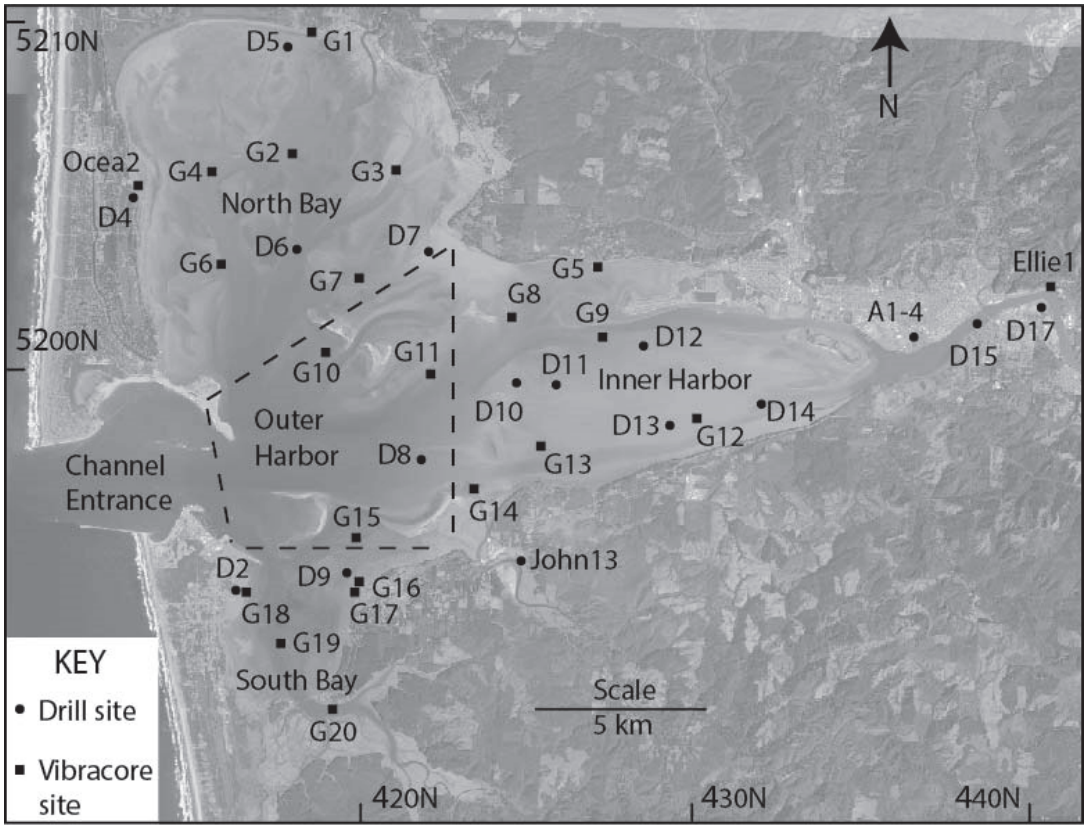

Figure 3. Map of drill site and continuous vibracore sites in Grays Harbor

Positions of numbered drill core sites (D and A), gouge core sites (Ocea2, Ellie1 and John13), and vibracore sites (G) are shown relative to modern tidal channels. Position data for drill core sites (Peterson & Phipps, 2016) are presented in Table **2**. Position data for gouge cores (Peterson et al., 2000; Peterson and Cruikshank, 2014) and for vibracores (this article) are presented in Table 3.

Table 2. Selected drill core sites in Grays Harbor.

Site Name	UTM_N (m)	UTM_E (m)	Modern depositional setting	Drill site surface (+-m MTL)	Deepest utilized sample depth (m MTL)
A1-4	5201500	436700	TM	-3.0	-13.2
D2	5193500	416500	TM	+0.5	-10.0
D4	5205200	413200	TM	-0.5	-12.5
D5	5209800	417800	TF	-1.0	-5.5
D6	5203700	418100	SC	-4.0	-12.5
D7	5203700	422100	TF	-1.5	-5.0
D8	5197500	422000	SC	-9.5	-12.5
D9	5194000	419800	TF	-1.5	-6.0
D10	5199800	424800	SC	-5.0	-11.0
D11	5199800	426000	SC	-6.0	-11.0
D12	5201000	428600	SC	-6.0	-12.0
D13	5198200	429400	SC	-5.5	-11.5
D14	5199300	431500	SC	-4.5	-10.5

D15	5201900	438500	TM	+0.5	-12.5
D17	5202300	440500	TM	+0.5	-12.0

Notes: Selected archaeology boreholes (A) and drill core sites (D) in Grays Harbor, respectively, as summarized from Phipps et al. (2015) and Peterson and Phipps (2016). Summary data include position (UTM Sector 10 T) in meters (m) northing (UTM_N) and easting (UTM_E), modern depositional setting, drill site (surface) elevation in meters (+-m) relative to mean tidal level (MTL), and deepest sample depth (m MTL) utilized for this study (0.5 m elevation resolution). Modern depositional settings are as follows, subtidal channel bank (SC), intertidal channel bank (IC), lower-intertidal flat (TF), and upper-intertidal marsh (TM).

Continuous vibracores (2–4 m depth) were collected in shallow lower intertidal sites (G) with an oyster dredge platform and hydraulic winch-out (Figure 3 and Table 3). Core site positions were established with GPS. Site surface elevations in the tidal flats and subtidal channels were estimated (0.5 m resolution) from measured water depths and predicted tide levels (WWWTide, 2017). Vibracores were cut to 1.5 m sections, drained, and split for scaled photography, visual logging, subsampling, and archival in core lab freezers. The hydraulic pull-out minimized vibracore disturbance, but resulted in some core bottom loss, resulting in core top gaps. Vibracores without top gaps were compared with measured subsurface penetration to yield estimated compaction or percent shortening. Measured compaction (n=15 vibracores) ranged from 3 to 12 % and averaged 7 %. Vibracore lengths are not expanded in this article, therefore basal radiocarbon age samples could be ~ 10 % deeper than reported.

Table 3. Vibracore and gouge core sites in Grays Harbor.

Site Name	UTM_N (m)	UTM_E (m)	Modern setting	Core top (+-m MTL)	Core length (m)	Shortening (%)
G1	5210200	418500	TM	+0.8	1.8	3
G2	5206640	418010	IC	-1.8	2.7	
G3	5206150	421090	TF	-1.6	3.8	5
G4	5206050	415550	TF	-1.0	4.0	8
Ocea2	5205550	413530	TM	+1.0	3.0	
G5	5203350	427160	TF	0.0	4.0	12
G6	5203260	415860	SC	-2.2	3.0	
Ellie1	5202950	440650	TM	+1.5	3.2	
G7	5202900	420070	TF/IC	-1.1	3.1	10
G8	5201800	424630	IC	-1.7	3.6	9
G9	5201320	427360	IC	-1.6	3.0	8
G10	5200650	419080	SC	-2.3	2.9	3
G11	5200070	422250	SC	-2.4	3.5	6
G12	5198860	430220	TF/IC	-0.2	3.9	
G13	5197950	425540	TF	-0.6	3.1	5
G14	5196630	423570	TF/IC	-1.2	2.9	7
G15	5195560	420070	IC	-0.6	4.0	7
John13	5194500	425500	TM	+1.3		
G16	5193790	420080	TF	-0.2	3.4	6
G17	5193700	420040	TF	-0.2	3.5	5
G18	5193450	416800	TM	1.0	3.3	
G19	5191940	417840	IC	-1.1	2.2	
G20	5189980	419410	IC	-0.8	2.3	11

Notes: Metadata for vibracore sites (G), and gouge core sites (Ocea2, Ellie1, John13) include positions (UTM Sector 10 T) in meters (m) northing (UTM_N) and easting (UTM_E), modern depositional settings, core top elevations in meters (m) relative to mean tidal level (MTL), and approximate core length (m), with compaction or length shortening (%) in representative cores. Modern depositional settings are as follows, subtidal channel bank (SC), intertidal channel bank (IC), lower-intertidal flat (TF), ocean-wave swept shoal (WS), and upper-intertidal marsh (TM). Tidal marsh profiles at sites Ocea2, Ellie1 and John13 are from Barnett (1997), Peterson et al. (2000) and Peterson & Cruikshank (2014).

Vibracore subsampling included channel-split samples (1 x 1 x 50 cm intervals) for sediment texture analyses, at 0.5 m intervals down-core. Analyses of sand source (river versus littoral) relied on augite:hypersthene counts (200 grains per sample at 250x) of sand in 0.062-0.25 mm size fraction (Scheidegger & Phipps, 1976; Peterson & Phipps, 2016) at 1.0 m intervals down-core in the continuous vibracores. Selected detrital wood and shell fragments were sampled from representative shallow vibracore sections for AMS radiocarbon analyses. Small-scale sedimentary structures generally included laminated mud, cross-bedded sand, and sand-mud couplets, but many sandy sections were disturbed by bioturbation, coseismic paleo-liquefaction, and/or compaction by vibracoring. Only the sand-mud couplets, indicative of accretionary bank deposition (Smith, 1988), are specifically identified in this article. Semi-continuous gouge core logs from three upper-intertidal sites (Figure 3) are from previous work (Barnett, 1997; Peterson et al. (2000) and Peterson & Cruikshank (2014). These three gouge cores, from representative tidal marsh/wetland sites, demonstrate coseismic subsidence events from Cascadia megathrust ruptures, as initially reported for the Grays Harbor study area by Atwater (1997). The three protected wetland records of coseismic subsidence at Ocea2, Ellie1, and John13 (Table 3), are used in this article for comparison to vibracore records of interpreted coseismic subsidence in Grays Harbor.

4. Results

In this section, late-Holocene deposits in Grays Harbor are described for depositional setting, quantitative sediment composition, and deposit interval age. Analyses from shallow subtidal channel deposits (≤10 m depth MSL) are summarized from previously reported drill core sites (Peterson & Phipps, 2016). Analyses from intertidal channel banks and intertidal flats are newly reported from continuous vibracore sections (2–4 m depth subsurface) presented in this article. These overlapping data sets are used to help constrain interpretations of depositional processes that have led to the development and maintenance of the shallow tidal channels and lower-intertidal flats in Grays Harbor during latest-Holocene time.

4.1 Deposit Compositions and Ages in Drill Core Sites

Sediment texture composition (% sand fraction), sand source (% littoral sand), and radiocarbon dates are compiled for the upper ~10 m elevation intervals (0 to -12.5 m MTL) of drill core sites in Grays Harbor (Figure 4**)** (Peterson & Phipps, 2016). With the exceptions of three shallow peripheral tidal flat sections in sites D5, D7 and D9 (Figure 3), and one tidal-riverine floodplain section at site D17, the drill core samples largely reflect subtidal channel deposition. The subtidal channel deposits are dominantly sand rich (≥75 % sand) and decrease in littoral sand abundance from dominantly littoral sand supply in the Outer Harbor sub-region to dominantly river sand supply in the landward-most reaches of the Inner Harbor sub-region. Drill core site D9 is an important exception to this trend with significant river sand components (40–60 % abundance) near the tidal inlet. Radiocarbon ages from four drill core sites (D6, D8, D15, and D17) at elevations of -11 to -12.5 m MTL range from 4.5 to 6.6 ka. Maximum historic channel depths of ~ 10 m occurred within the vicinity of the dated drill core sections (USCGS, 1973), so the deeper dated sections (-10 to -12.5 m MTL) are thought to reflect channel bottom or near bottom ages. The subtidal channel deposits were largely derived from lateral migration(s) of major channels that occurred at multi-millennial time scales in Grays Harbor. Deposit compositions and ages from the smaller lower-intertidal channels (-2 to 0 m MTL) and intertidal flats (~0±1.5 m MTL) in Grays Harbor are presented below.

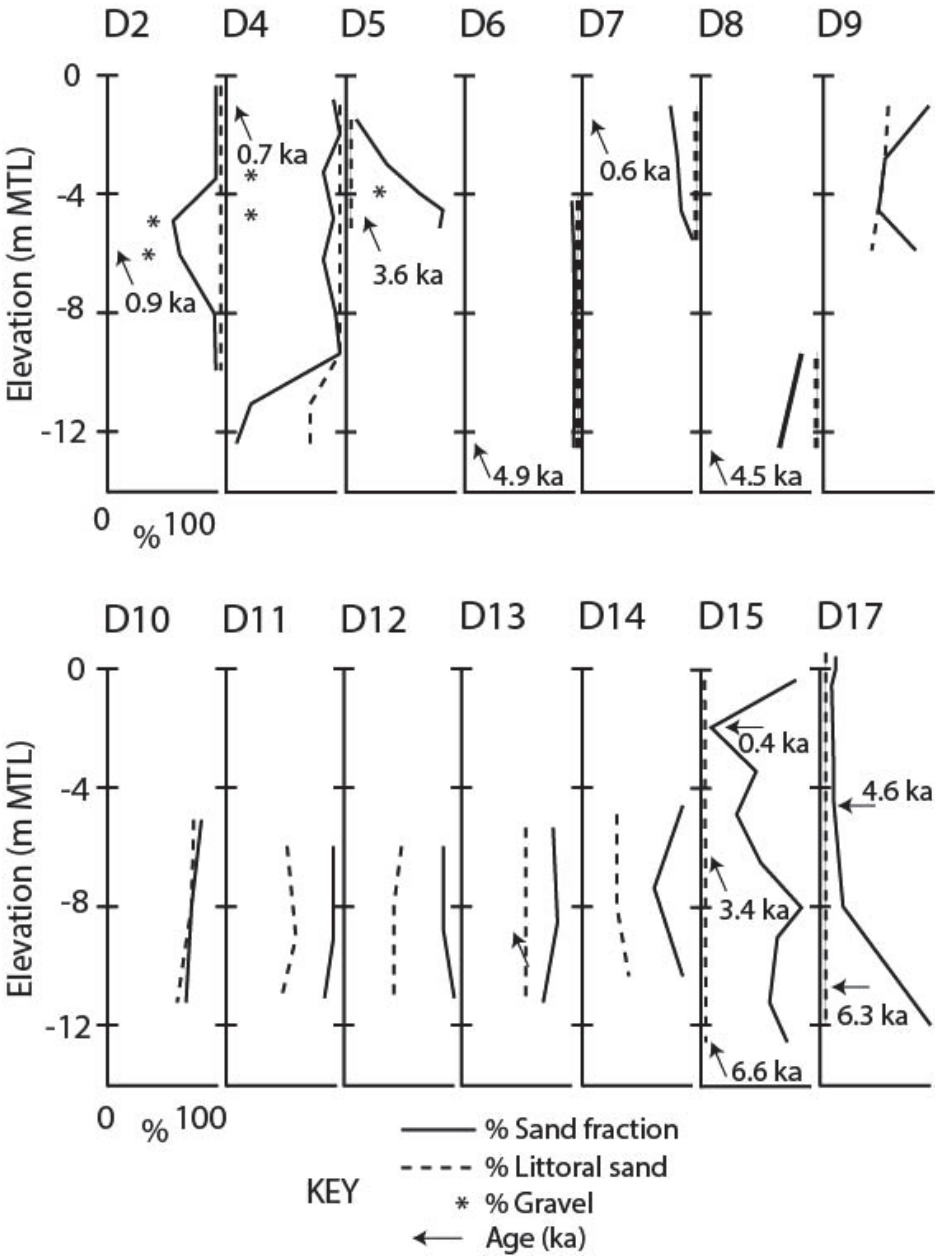

Figure 4. Plots of sediment composition and age from selected drill core site intervals in Grays Harbor

Sediment grain size (percent sand abundance relative to mud or gravel*), sand source composition (percent littoral sand), and reported radiocarbon ages (ka) are shown for selected drill core site intervals (≤12.5 m MTL) in Grays Harbor (Peterson & Phipps, 1992; Peterson & Phipps, 2016). ^{14}C age data in calibrated years BP are presented in Table 5. Analyses of deeper samples (10–60 m depth) can be found in Peterson & Phipps (2016). See Figure 3 for drill site (D) locations in Grays Harbor, with site numbers increasing from west to east, at increasing distances from the tidal inlet.

4.2 Deposit Facies Sequences in Continuous Vibracores and Gouge Cores

Vibracore logs of sediment composition from the northern areas of Grays Harbor are shown in Figure 5. Vibracores G1, G3, G4, and G5, in marginal tidal flats, record several events of upper-intertidal marsh or mud flat burial by lower-intertidal sand flat deposits (Figure 6). Such records of tidal flat response to abrupt submergence by coseismic subsidence are widely distributed in broad marginal tidal flats in nearby Willapa Bay (Figure 1) (Peterson & Vanderburgh, 2018). The coseismic subsidence events in the central and lower Grays Harbor (1±0.5 m relative sea level rise) are regionally correlated by depth and ^{14}C age in protected tidal marsh settings, such as

Ellie1 (Atwater, 1992), and by corresponding paleotsunami sand sheets in the lower estuarine reaches (Ocea2) (Peterson & Cruikshank, 2014) (Figure 3). The youngest coseismic subsidence event (Y) is regionally correlated to the last Cascadia megathrust rupture in AD 1700 (Stake et al., 1996; Atwater et al., 2004). It is not known whether fewer numbers of apparent submergence events recorded in sites G3 and G4 (n events=1 or 2) compared to Ocea2 and Ellie1 (n events=4 each) for equivalent depth intervals reflect incomplete recording or poor preservation of coseismic subsidence event records in the high-energy tidal flat settings. Sand deposits that grade up-core to mud and sand couplets in vibracore G2 are interpreted to represent vertical accretion from subtidal to intertidal channel deposits (Smith, 1988). A thick sand sequence (~3 m thickness) in vibracore G6 is representative of subtidal channel bank deposition. Modern sand wave bedforms have been documented in subtidal channel bottoms of the Grays Harbor channel entrance and Outer Harbor sub-region by acoustic profiling (Peterson & Phipps, 1992). The nearly-symmetric sand waves that were observed in those major channels demonstrate strong bi-directional tidal flow in the modern sandy channel bottoms.

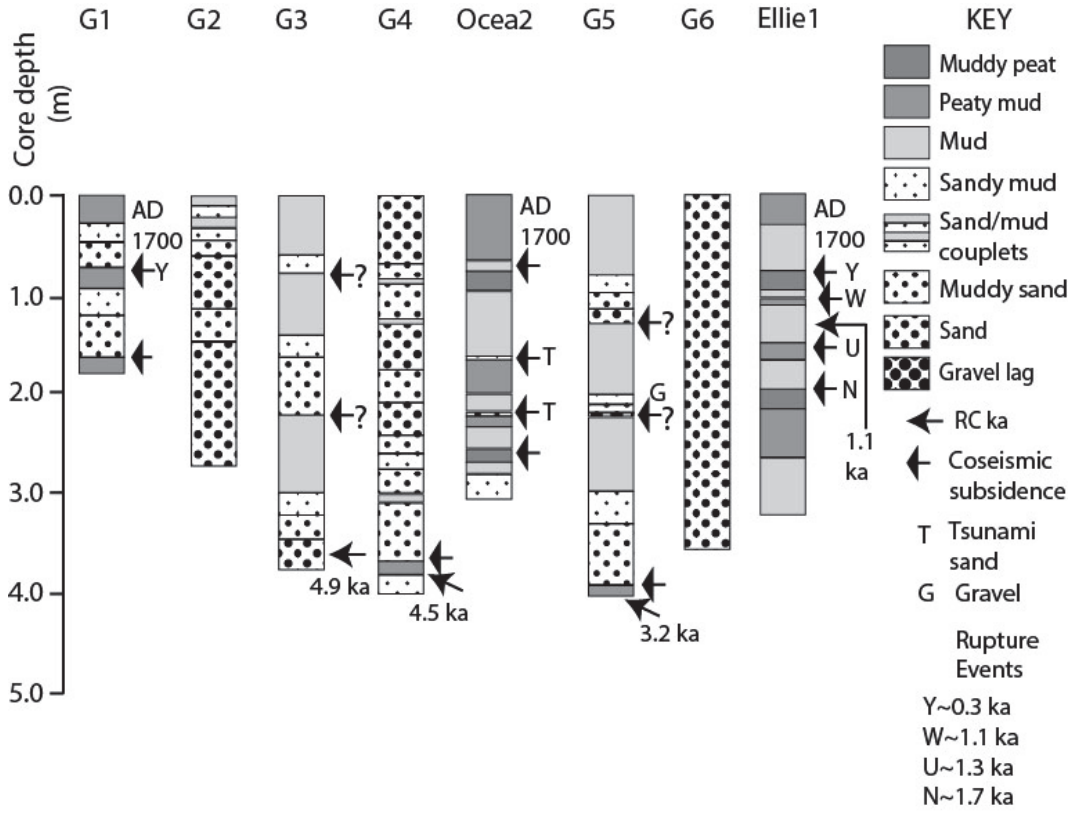

Figure 5. Core logs from vibracores (G) and gouge cores (named) in Grays Harbor

Core depths (m) are subsurface. Core site settings and locations are summarized in Table 2 and Figure 3. Radiocarbon ages for vibracore sites are shown in Table 5. The radiocarbon date for the Ellie locality is from Atwater (1992). The lettered rupture events (Y, W, U, N) and estimated ages for Ellie1 are correlated from Atwater (1997). The measured section (Ellie1) is from Peterson & Cruikshank (2014). The first subsidence events in Ocea2 and G1 are taken to be from the last Cascadia rupture (event Y) at AD 1700 (Satake et al., 1996; Atwater et al., 2004).

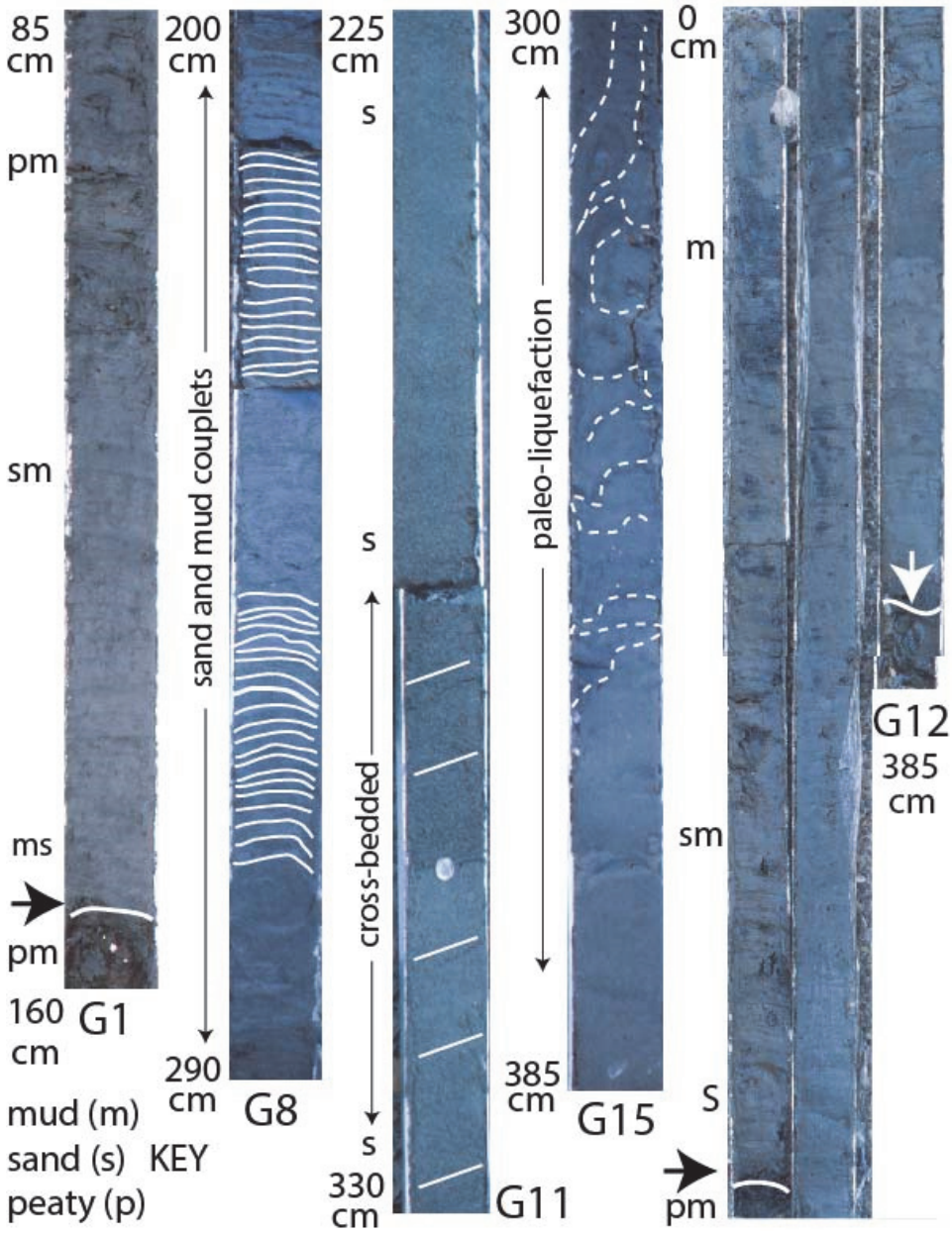

Figure 6. Photos of vibracore sections

Sections of vibracores G1 (0–160 cm depth subsurface), G8 (200–290 cm depth), G11 (225–330 cm depth), G15 (300–385 cm depth) and G12 (three sections of 0–150 cm, 150–300 cm, and 300–385 cm depth, left to right). Buried peaty muds (black arrows) represent coseismic subsidence events in G1 and G12. Sand and mud couplets (200–290 cm depth) in vibracore G8 represent lower-intertidal accretionary bank deposits. Sand (225–330 cm depth) in vibracore G11, with some cross-bedding on either side of a coin, represents subtidal accretionary bank deposits. Clastic sand sills and sand dikes (dashed white lines) above structure-less sand (365–385 cm depth) in vibracore G15 represent paleo-liquefaction, probably of coseismic origin. Vibracore G12 contains a basal gravel layer (white arrow), overlain by sand and muddy sand (320–385 cm depth), overlain by sand and mud couplets (180–320 cm depth), overlain by peaty mud (150-180 cm depth), buried by sand and muddy sand (30–150 cm depth), which grade upward to mud at the core top.

Vibracore logs from the middle areas of Grays Harbor are shown in Figure 7. Vibracores G8 and G9 are from lower-intertidal channel banks (Figure 3 and Table 3). They include sand and mud couplets and muddy sand layers, which are distinctive for intertidal channel accretionary banks (Figure 6). Vibracore G12 contains gravel from a

channel lag deposit at 3.8 m depth subsurface, which is overlain by sand-mud couplets of lower-intertidal accretionary bank deposits. The accretionary bank deposits transition up-core to a peaty mud reflecting a tidal marsh. The peaty mud was abruptly buried (sharp upper contact) by sand and muddy sand, representing coseismic subsidence and burial of the tidal marsh. Vibracores G13 and G14 include distinctive peaty mud or mud layers that were abruptly buried (sharp contacts) by sandy deposits, possibly reflecting coseismic subsidence events. One section at ~1.5 m subsurface depth in vibracore G8 might represent coseismic subsidence of an intertidal accretionary bank. Vibracores G7, G12, and G14 are from modern tidal flats, but are from positions that are close to modern tidal channel banks. Vertical sequences in those three vibracores suggest up-core transitions from lower-intertidal accretionary bank settings, including sand and mud couplets, to finning-up tidal flat settings, including alternating sand and mud layers. Thick sand sections (~ 3.0 m) in vibracores G10 and G11 likely developed in subtidal channel bank settings.

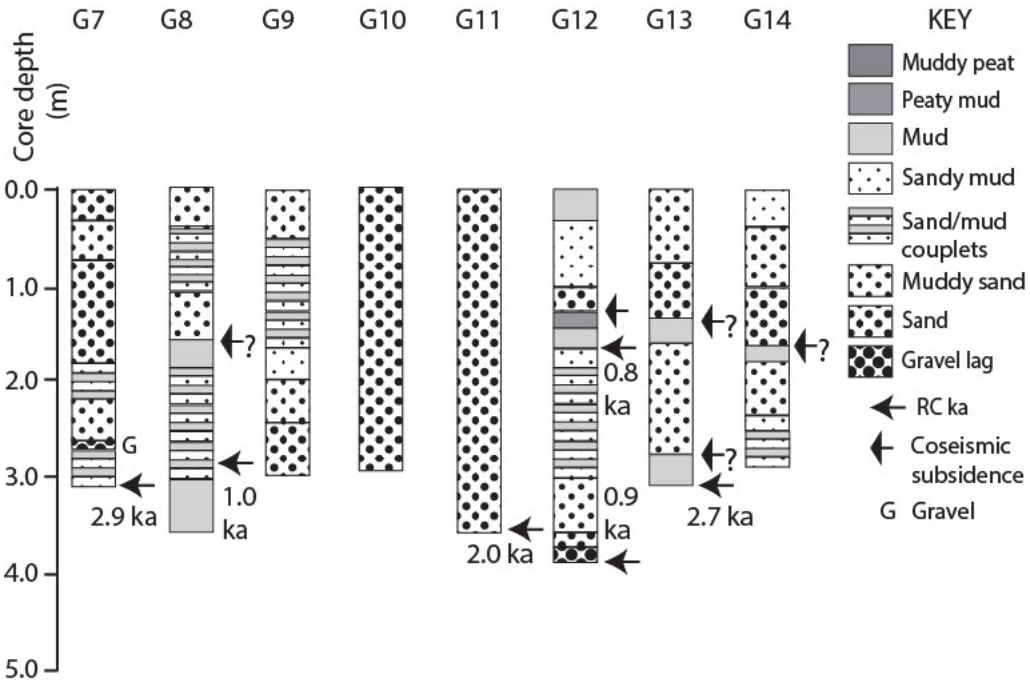

Figure 7. Core logs from vibracores in Grays Harbor estuary

Core depths (m) are subsurface. Core site settings and locations are summarized in Table 2 and Figure 3**.** Radiocarbon ages for vibracore sites are shown in Table 5.

Vibraore logs from the southern areas of Grays Harbor are shown in Figure 8. Sand and mud couplets and muddy-sand sediments in vibracores G15, G19 and G20, are consistent with accretionary bank deposits in lower-intertidal channel settings (Figure 3 and Table 3). Sand sills and dikes disrupt bedding between 3.0 and 4.0 m depth in vibracore G15. Overlying sand and mud couplets at 2.7 m depth and 2.0–1.0 m depth in vibracore G15 were not disturbed, indicating a paleo-liquefaction event at depth in G15. Sand and mud couplets or intertidal accretionary bank deposits in vibracores G15 and G17 are overlain by tidal flat sand and mud. Tidal flat sequences are interpreted to overlie subtidal channel deposits of sand in sites G16 and G18. Tidal marsh progradation over the tidal flat sequence in vibracore G18 (< 1.5 m depth subsurface) records the last regional coseismic subsidence event at AD 1700. No paleotsunami sand deposits were observed at buried wetland horizons at site John13 (Barnett, 1997), located in a protected tidal creek marsh in the central reaches in Grays Harbor. An anomalous gravel layer was recorded in tidal flat deposits in vibracore G17, located in the northeast corner of the South Bay sub-region. It is not known whether that anomalous gravel layer (3 cm thickness) represents paleotsunami surges in the South Bay channel. However, a lack of apparent paleotsunami sand deposition in the more distal sites that do record coseismic subsidence events (John13 and Ellie1) suggest dissipation of paleotsunami surges over the shallow tidal flats of the Inner Harbor sub-region.

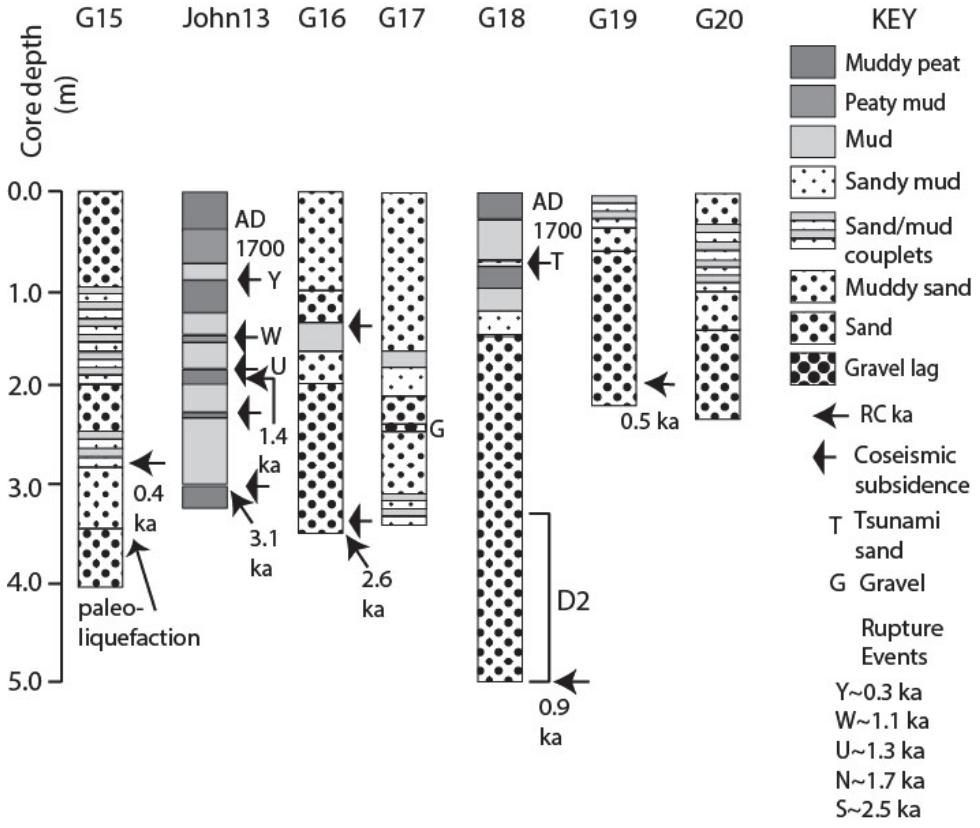

Figure 8. Core logs from vibracores (G) and gouge cores (named) sites in Grays Harbor

Core depths (m) are subsurface. Core site settings and locations are summarized in Table 2 and Figure 3**.** Radiocarbon ages for vibracore sites are shown in Table 5. The radiocarbon date for the John locality is from Atwater (1992). The measured section (John13) is from Barnett (1997) and Peterson & Cruikshank (2014). The lettered rupture events (Y, W, U, N, S) and estimated ages for John13 are correlated from Atwater (1997). The first subsidence event in vibracore site (G18) is taken to be from the last Cascadia rupture (event Y) at AD 1700 (Satake et al., 1996; Atwater et al., 2004).

4.3 Grain Size and Sand Source Compositions in Vibracore Samples

Grain size fractions in the recovered vibracore sections include sand and mud, with gravel representing less than 1% in the channel-split samples (50 cm in length), as taken at 0.5 m intervals down-core (Table 4). Large shells or shell fragments, potentially grown or burrowed in-situ, were removed by hand prior to grain-size analyses. The sand fraction (62-2000 µm settling equivalence) ranges from 6 to 100 percent (Table 4) with a total sample (n=124) mean and 1 standard deviation of 71±28 1σ percent sand. Sand mean grain sizes range from 109 to 265 µm with a total sample (n=124) mean and 1 standard deviation of 175±x34 1σ µm sand grain size.

Littoral and river sand abundances, as based on hyperthene:augite endmember ratios of river=0.06 and beach or littoral=0.83 (Peterson and Phipps, 2016) are presented to the nearest percent (Table 4), but replicate slide counts yield several percent variability. Compositions are shown as percent littoral sand with the balance representing the river sand component (Table 4). Littoral sand abundances range from 100 % to 0 %, with a mean and standard deviation for all samples (n=67) of 60±35 1σ % littoral sand. Littoral sand abundance decreases with increasing distance from the channel entrance, as expected (Scheidegger & Phipps, 1976; Peterson & Phipps, 2016). However, several vibracore samples from sites in the Outer Harbor sub-region (sites G11, G15, G16 and G17) contained anomalous, or higher than expected, abundances of river sand (20–30 %) in some core sections, as explained in Section 4.4 below.

Table 4. Vibracore sediment grain size distributions and sand source components.

Site	0-0.5 m	0.5-1.0 m	1.0-1.5 m	1.5-2.0 m	2.0-2.5 m	2.5-3.0 m	3.0-3.5 m	3.5-4.0 m
G1	19 %S 137±73 0 %L	43 %S 113±45	56 %S 175±19 0 %L	31 %S 165±35				
G2	71 %S 154±40 5 %L	76 %S 173±35	87 %S 170±35 7 %L	95 %S 169±28	97 %S 169±25 11 %L			
G3	32 %S 135±75 14 %L	37 %S 133±58	39 %S 144±51 15 %L	53 %S 140±47	57 %S 180±66 11 %L	7 %S 148±71	68 %S 167±61 12 %L	
G4	80 %S 167±36 31 %L	90 %S 166±30	76 %S 159±36 28 %L	90 %S 163±33	77 %S 164±31 34 %L	27 %S 159±62	89 %S 169±34 33 %L	40 %S 152±37
G5	6 %S 120±45 NA %L	30 %S 146±65	73 %S 138±40 18 %L	9 %S 123±49	27 %S 139±61 13 %L			
G6	95 %S 174±32 81 %L	94 %S 181±35	98 %S 174±29 78 %L	98 %S 172±29	98 %S 177±31 82 %L	95 %S 191±48	97 %S 175±32 87 %L	
G7	95 %S 186±35 86 %L	76 %S 180±33	97 %S 189±36 92 %L	97 %S 182±32	79 %S 181±334 85 %L	55 %S 170±36	19 %S 164±65 89 %L	
G8	41 %S 141±73 27 %L	50 %S 149±67	63 %S 165±57 25 %L	63 %S 154±52	47 %S 163±55 28 %L			
G9	53 %S 146±59 28 %L	46 %S 150±53	43 %S 139±45 19 %L	65 %S 177±35	81 %S 184±47 26 %L	87 %S 169±38		
G10	96 %S 204±33 97 %L	98 %S 189±32	98 %S 194±47 98 %L	98 %S 190±45	98 %S 200±49 100 %L			
G11	95 %S 198±29 99 %L	96 %S 221±31	221 %S 210±37 93 %L	96 %S 181±34	99 %S 168±24 69 %L	97 %S 189±36	97 %S 182±32 84 %L	
G12	21 %S 109±52 14 %L	26 %S 122±65	73 %S 158±38 17 %L	17 %S 129±60	60 %S 142±40 21 %L	30 %S 115±49	45 %S 149±45 16 %L	60 %S 170±54
G13	68 %S 174±43 46 %L	97 %S 180±34	97 %S 175±32 48 %L	78 %S 172±40	84 %S 170±41 43 %L			
G14	58 %S 175±59 89 %L	80 %S 248±191	84 %S 357±188 90 %L	86 %S 345±146	57 %S 184±121 62 %L	33 %S 150±67		
G15	95 %S 204±36 85 %L	97 %S 179±32	65 %S 159±54 98 %L	66 %S 163±45	92 %S 180±37 87 %L	80 %S 178±39	89 %S 200±50 72 %L	96 %S 199±35
G16	84 %S 197±37 88 %L	80 %S 198±31	87 %S 179±47 100 %L	54 %S 151±53	95 %S 231±65 89 %L	91 %S 265±188	98 %S 200±45 78 %L	97 %S 187±27
G17	72 %S 184±61 91 %L	82 %S 199±60	88 %S 204±59 100 %L	98 %S 185±32	98 %S 214±50 85 %L	83 %S 174±52	22 %S 147±43 67 %L	
G18	7 %S 120±38 NA %L	9 %S 162±49	15 %S 176±59 100 %L	97 %S 202±47	97 %S 204±43 94 %L	98 %S 195±35	98 %S 185±32 96 %L	

G19	80 %S	95 %S	95 %S	96 %S	96 %S
	170±56	174±48	177±37	183±32	185±35
	95 %L		93 %L		97 %L
G20	57 %S	24 %S	73 %S	93 %S	95 %S
	162±42	168±57	184±42	179±35	217±47
	91 %L		86 %L		88 %L

Notes: Channel-split samples (1 cm width, 1 cm depth and 30–50 cm length) taken at 0.5 m intervals from 0 m to 4 m depth below surface. Large shell fragments (>0.5 cm diameter) were removed by hand from the sample prior to grain-size fraction analyses by wet sieving. Grain size fractions sand:mud are shown as percent weight sand (%S) >62 μm screen mesh size. Gravel (>2000 μm) was absent above trace levels (< 1 %) in all but a few samples. The sand size fractions were analyzed for grain size mean (μm) and standard deviation (mean ± 1 σ μm) based on settling equivalence in glycol, using a Sedigraph ™. The 62–250 μm fine sand size fraction was analyzed for percent littoral (%L) sand source, based on hypersthene (beach): augite (river) ratios in the non-opaque colored heavy-mineral fraction (Peterson & Phipps, 2016). Very-small amounts of the sand size fraction in some mud samples were not analyzed (NA).

4.4 Vertical Trends of Deposit Textural and Sand Source Compositions in Vibracores

Grain size distributions, represented by sand fraction percent (sand %), vary substantially between some vibracore depth sections, taken at 0.5 m intervals down-core (Figures 9 and 10). These deposit textural changes follow the facies vertical trends that are shown in Figures 5, 7 and 8. The quantitative measurements of sand versus mud confirm dramatic changes in depositional energy, apparently associated with 1) transitions between channel and tidal flat environments and 2) neotectonic cycles of aseismic uplift and coseismic subsidence. Sand sources, presented as percent littoral sand (littoral %), are generally consistent between 1.0 m vertical sections within the shallow vibracores. Local sand source mixing was relatively uniform within vibracore site localities regardless of transitions between tidal channel and tidal flat depositional settings. Several vibracore core sites (G11, G15, G16, G17), in the littoral sand-rich Outer Harbor sub-region (Figure 3), show anomalous river sand abundances (up to 20–30 % total abundance) in some depth intervals. Evidence of river sand transport to the lowest estuarine reaches in Grays Harbor was unexpected, based on modern sample analyses (Scheidegger & Phipps, 1976). In retrospect, a suggestion of such seaward river sand transport was provided by substantial river sand components in drill core site D9 (Figure 4) located just south of the Outer Harbor sub-region (Figure 3). The significance of these findings is discussed further in Sections 5.1 and 5.6 below.

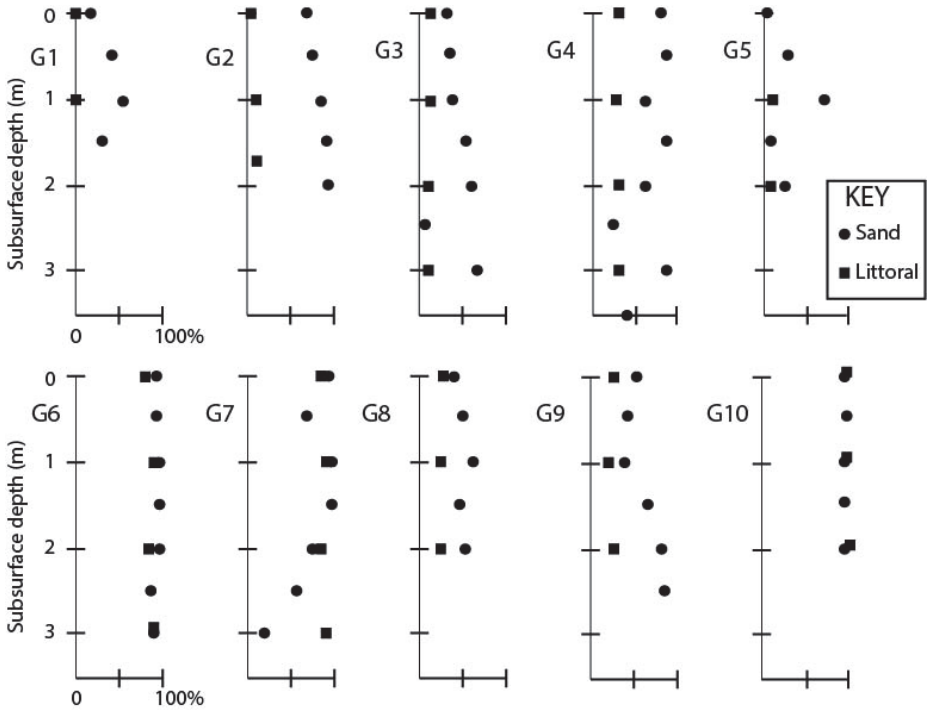

Figure 9. Plots of deposit composition in vibracores from Grays Harbor

Sediment sample compositions including percent sand (sand) and percent littoral sand (littoral), respectively, are shown at 0.5 m and 1.0 m intervals down-core. See Table 4 for quantitative data.

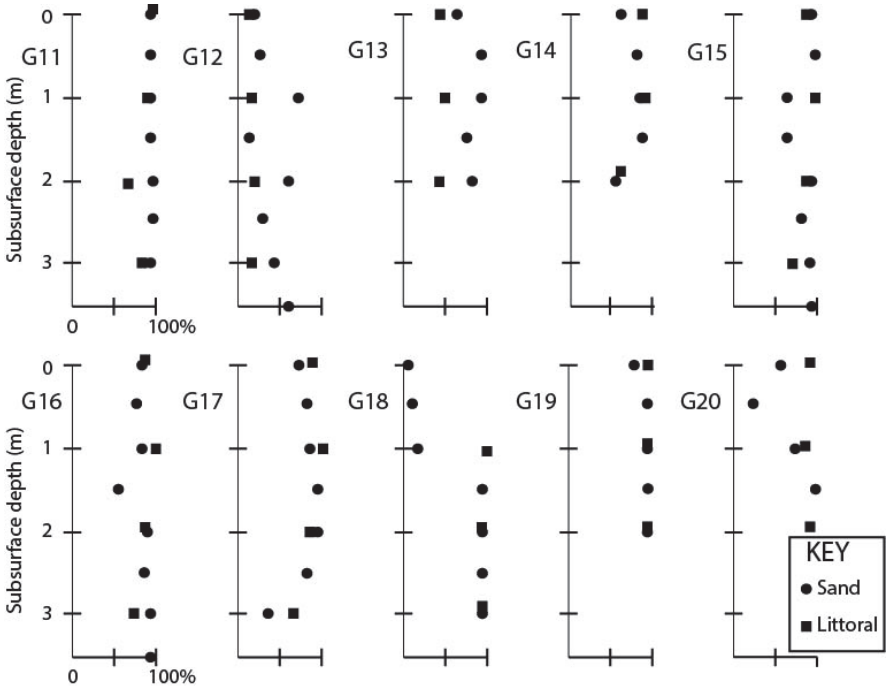

Figure 10. Plots of deposit composition in vibracores from Grays Harbor

Sediment sample compositions including percent sand (sand) and percent littoral sand (littoral), respectively, are shown at 0.5 m and 1.0 m intervals down-core. See Table 4 for quantitative data.

4.5 Drill Core and Vibracore Deposit Sample Ages

^{14}C Sample ages from selected drill core sites (D), hollow-stem auger sites (A), and from new vibracore sites (G) are shown in Table 5. The available sample ages and depths are used to construct sea level and sediment level curves for Grays Harbor in late-Holocene time (see Section 4.6 below). In addition to 26 ^{14}C sample ages, three modern marsh tops (0 ka in age) are included to constrain the sea level curve during latest-Holocene time. The ^{14}C dated deposits range in age from 400 to 6,579 median probability calibrated years BP. The mean and standard deviation of the compiled ^{14}C median probability ages (n=26) are 2,719±2,019 ±1σ calyrBP.

Table 5. Grays Harbor shallow drill core, vibracore and wetland gouge core sample ages.

Site	Core depth (m)	Elevation (-m) MTL	Material/ Method	Convention yrBP ±1σ	Calibrated calyrBP±2σ	Median yrBP	Beta Analytic #
D5	4.0	-5.0	Wood	3380±80	3449–3835	3628	20309
G3	3.6	-5.2	Wood/AMS	4310±60	4652–5211	4894	158076
Ocea2	0	+1.0	Marsh top			0	
G4	3.9	-4.9	Peaty/AMS	4000±60	4256-4798	4479	158074
D4	0.5	-1.0	Peaty	830±60	671–907	753	2093
D6	8.5	-12.5	Shell	5080±90	4694–5251	4940	20528
D7	0.5	-1.5	Wood	620±70	523–677	600	20308
G5	4.0	-4.0	Peaty	3030±30	3145-3344	3230	495778
G7	3.1	-4.2	Organics	2780±30	2793-2952	2877	495779
Ellie1	0	1.5	Marsh top			0	
Ellie1	1.3	+0.2	Organics		951-1259		
D17	5.0	-4.5	Peaty	4120±80	4438–4488	4651	20529
D17	11.5	-11.0	Peaty	5540±80	6185–6495	6342	20530
G8	2.9	-4.6	Wood/AMS	1130-±40	960–1174	1035	158081

D15	2.5	-2.0	Wood	330±100	255–540	376	20296
D15	7.0	-6.5	Wood	3190±230	2809–3973	3403	20297
D15	13.0	-12.5	Peaty	5770±140	6293–6893	6579	20527
A1	7.0	-10.0	Peaty	4950±40	5597–5824	5677	264293
A2	5.0	-8.0	Wood	1130±40	960–1174	1035	263291
A4	6.9	-9.9	Wood	1000±40	796–975	919	263290
G11	3.5	-5.9	Organics	2040±30	1923-2068	1995	495780
G12	1.4	-1.6	Wood/AMS	900±50	726–926	823	158082
G12	3.9	-4.1	Wood/AMS	950±40	768–934	855	158080
G13	3.1	-3.7	Organics	2620±30	2380-2717	2752	495781
John13	0	+1.3	Marsh top			0	
John13	1.8	-0.5	Peaty		1296-1529		
John13	3.1	-1.8	Peaty			3,200*	
D8	3.0	-12.5	Shell	4740±100	4214–4799	4493	20301
G15	2.8	-3.4	Shell	750±40	NA	400**	158077
G16	3.4	-3.6	Organics	2470±30	2380-2717	2578	495782
D2	5.5	-5.0	Shell	1360±70	737–1057	903	20279
G19	2.0	-3.1	Wood/AMS	440±50	319–544	491	158084

Notes: Calibrated radiocarbon ages are from Calib 7.10 online (Calib7.10, 2017) using IntCal13 and MARINE13 for shell materials (Stuiver, et al., 2017). Shell sample delta R values (Delta R=392 yr error +/- 35 yr) are from Yaquina Bay, Oregon (Robinson, 1981). *John13 subsidence at 3.1 m depth subsurface was correlated by Atwater to regional subsidence at 3.2 ka (Atwater et al., 2004). **G15 shell sample at 2.8 m core depth yielded a marine reservoir corrected radiocarbon age of ~400 yr. ^{14}C sample ages from selected drill core sites (D) are from Peterson & Phipps (2016). ^{14}C sample ages from hollow-stem auger sites (A) are from Phipps et al. (2015). ^{14}C sample ages from gouge sites (Ellie and John13) are from Atwater (1992) as calibrated by Peterson & Cruikshank (2014). ^{14}C sample ages from vibracore sites (G) are newly reported here. See Figure **3** for site locations, and Tables 2 and **3** for site position data.

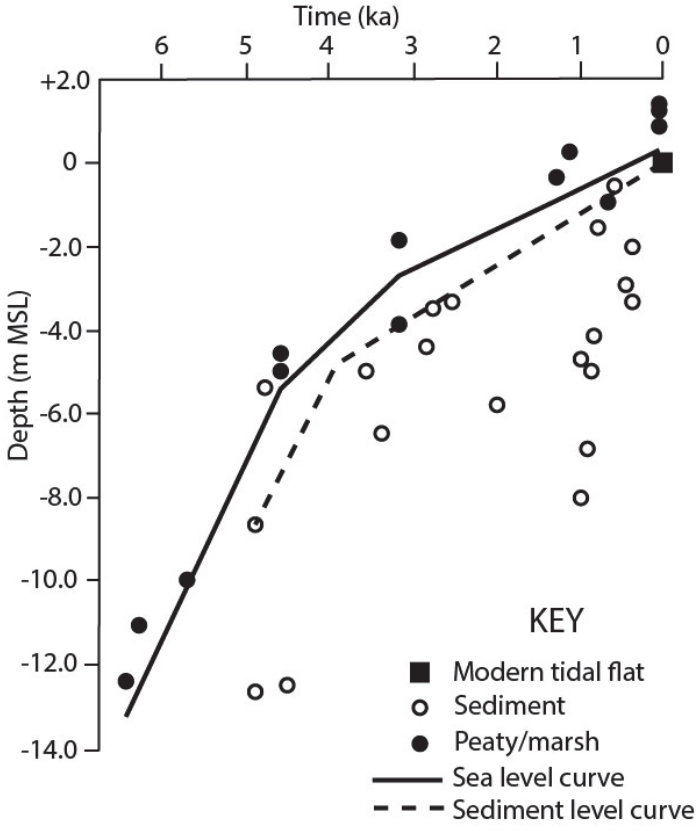

Figure 11. Plot of sea level and sediment level curves

4.6 Sediment Level and Sea Level Curves

The dated sediment deposits (n=31) from Table 4 are plotted for age (ka) and depth (m MTL) in Figure 11. The deposit depth and age relations are interpreted in terms of sea level and sediment level curves. Modern and paleo-tidal marsh deposits are used to establish paleo-tidal levels or mean sea levels during late-Holocene time. Modern tidal marshes occur between 0.5 and 1.5 m MTL in Grays Harbor (Barnett, 1997; Peterson et al., 2000). Forested wetlands, yielding tree roots and stumps, generally occur at supratidal elevations, above 1.5 m MTL. Barren mud and sand deposits generally occur below 0.5 m MTL. Peaty deposits, representing paleo-tidal marshes serve as proxies for paleo-tidal levels (1±0.5 m paleo-tidal level resolution) in Grays Harbor. Therefore, mean paleo-tidal levels or mean paleo-sea levels are taken to be ~1.0 m below corresponding peaty mud deposits. Within latest-Holocene time, or during the last ~3.0 ka, the rate of sea level rise in Grays Harbor is estimated to be ~1.0 m ka^{-1}.

Estimated sea level (bold line) and sediment level (dashed line) curves, respectively, are plotted from ^{14}C dated peaty deposits (tidal marshes) and siliclastic sediment deposits in Grays Harbor. Data are from Table 5. Paleo-tidal levels (sea levels) are taken to be 1.0 m below corresponding paleo-tidal marsh deposits (solid circles). Modern intertidal flat elevation data (solid square) are averaged from 5 tidal marsh core sites and 9 lower-intertidal flat sites (Table 3) which average 0±0.9 1σ m MTL (n=14). The sediment level curve is drawn to represent the average upper-limit of intertidal flat deposition in Grays Harbor. Dated sediment deposits that fall well below the upper sediment level curve are thought to represent channel cut-and-fill sequences.

Dated mud and sand deposits (Table 5**)** represent dated paleo-deposit surfaces. Modern un-vegetated deposit surfaces in Grays Harbor range from 0.0 m MTL, at vibracore site G5 in a protected Inner-Harbor mud flat, to -9.5 m MTL at drill site D8, in a major subtidal channel axis in the Outer Harbor sub-region (Tables 2, 3 and Figure 3). For the purposes of this article averages of the highest un-vegetated deposits, for a given age interval, are used to establish the upper sediment level curve for Grays Harbor (Figure 11). During late-Holocene time the average upper limit of tidal flat deposition kept pace with rising sea levels in Grays Harbor. However, many of the dated sediment deposits shown in Figure 11 fall well below the upper sediment level curve for equivalent deposit ages. They are thought to reflect channel cut-and-fill sequences in the basin fill, as discussed in detail below. A potential bias in young (~1 ka) channel cut-and-fill deposit ages could have occurred in this study of latest-Holocene deposits (≤3 ka), due to core site proximity to modern tidal channels that provided access for rotary drilling and vibracoring from vessels anchored within, or adjacent to, the tidal channels (Figure 3).

5. Discussion

In this section, the latest-Holocene deposits in Grays Harbor are discussed in terms of depositional settings, sediment compositions, and associated sedimentation rates. The potential interactions of sediment supply, transport, and accommodation space limitations in shallow tidal channel and tidal flat depositional environments are explored to explain the long-term maintenance of the lower-intertidal flat settings in Grays Harbor. Though buffered against small changes in sediment supply and sea level rise, those lower-intertidal settings, which are important to migratory bird feeding, shellfish industries, and other ecosystem functions, could be vulnerable to future anthropogenic impacts.

5.1 Latest-Holocene Deposit Compositions, Facies Sequences, and Sedimentation Rates

The quantitative textural compositions of channel fill and tidal flat deposits in Grays Harbor (Figures 4, 9 and 10) are summarized for the estuary sub-regions in Table 6. Sub-region deposit compositions are calculated from averages of core site samples from drill core sites and virbracore sites. The site averages, based on samples from between 0 and -3.5 m depth subsurface, were then averaged for each sub-region. No core samples were obtained from the Channel Entrance sub-region due to strong currents and high ocean wave energy in the tidal inlet. The two core sites located nearest to the Channel Entrance sub-region, D2 and G18 (Figure 3), were used to estimate compositions for the tidal inlet area. The sub-region deposit compositions, including relative percent sand size fraction, littoral sand, river sand, and mud, were multiplied by surface area (Table 1) to yield deposit component volumes, as normalized to 1.0 m depth. The littoral sand volumes, as normalized to 1.0 m depth interval, ranged from 40 x 10^6 m^3 in the Outer Harbor sub-region to 13 x 10^6 m^3 in the Inner Harbor sub-region. The river sand volumes ranged from 30 x 10^6 m^3 in the Inner Harbor sub-region to 0.4 x 10^6 m^3 in the Channel Entrance sub-region. The river mud volumes ranged from 23 x 10^6 m^3 and 24 x 10^6 m^3, respectively, in the Inner Harbor and North Bay sub-regions, to 0.6 x 10^6 m^3 in the Channel Entrance sub-region.

Table 6. Sub-region and total basin averaged sediment compositions and volumes per one meter depth interval.

Sub-region	Sand size fraction (%)	Sand size mean (μm)	Littoral sand (%)	Littoral sand volume (m^3)	River sand volume (m^3)	River mud volume (m^3)
Channel Entrance	96*		98*	15×10^6	0.4×10^6	0.6×10^6
Outer Harbor	94	190	93	40×10^6	3×10^6	3×10^6
North Bay	72	163	52	33×10^6	30×10^6	24×10^6
South Bay	77	191	87	15×10^6	3×10^6	5×10^6
Inner Harbor	62	164	36	13×10^6	24×10^6	23×10^6
Total				117×10^6	60×10^6	55×10^6

Notes. Data are averaged for 0–3 m depth (subsurface) intervals in drill core sites (Figure 4) as reported in Peterson & Phipps (2016) and for all measured vibracore depth intervals, which average ~3 m depth subsurface (Table 4). Channel entrance sediment compositions (*) are taken from the closest available site sections, including the upper three meters of D2 and the bottom two meters of G18. The averaged core site data are compiled and averaged for each sub-region. The averaged sub-region data are compiled and averaged for the basin total (Total). Sediment volume data for the sub-regions are calculated from 1) averaged compositions, including sand size fraction %, mud fraction %, littoral sand % of the sand size fraction, and river sand % of the sand size fraction, 2) sub-region surface areas (Table 1), and 3) are normalized 1.0 m depth intervals.

Several basin-wide compositional trends stand out from Table 6. Even though several substantial rivers enter Grays Harbor (Figure 2) the total basin volume of littoral sand is nearly twice the size of the river sand volume. What mechanisms could account for such an efficient import of littoral sand into the mesotidal estuary? The volume of river sand is approximately equal to the river mud volume, even though the supply of river bedload (primarily sand) is thought to be three times smaller than the supply of suspended river sediment (silt and clay) to Grays Harbor (Peterson & Phipps, 2016). What mechanisms could have been responsible for the effective winnowing and export of river mud out of Grays Harbor? These questions are addressed in Sections 5.4 and 5.5 below.

Shallow tidal channels imported both sand and mud into the estuary, but largely exported mud out of the estuary. Floodplain-constricted fluvial-tidal channels conveyed river sediments, mud and sand, into the upper estuarine reaches (Figure 2**)** as represented by drill site D15 (Figure 4). In the lower estuarine reaches sand-bottomed subtidal channels, as represented by drill site D8, imported littoral sand into the central reaches of the estuary, presumably by near-bottom sand transport. These same sub-tidal channels in the Outer Harbor and Channel Entrance sub-regions were the conduits by which mud was exported out of Grays Harbor, under suspension transport. Export of the suspended mud fraction might have benefitted from the small salinity gradient and slight density stratification in Grays Harbor (Barrick, 1976). However, the weak density-driven bottom 'in-flow' would likely have been insufficient to account for the landward transport of littoral sand into the central estuarine reaches, as the shallow tidal channels in Grays Harbor are partially- to well-mixed (Barrick, 1976). Slight asymmetries in flood and ebb tidal flow velocities and/or durations lead the net-landward advective transport of littoral sand into the North Bay, South Bay and Inner Harbor sub-regions.

A small, but important, exception to the net landward bottom transport of littoral sand in the lower reaches of Grays Harbor is evident from the minor river sand components (20–45 %) in drill core samples from site D9 and in some vibracore sections from sites G15, G16, and G17, all located on the south side of the Outer Harbor sub-region (Figure 3). The minor river sand components in some pre-historic core intervals (Tables 4 and 5), demonstrate episodes of ebb-dominated bottom flow on the south side of the Outer Harbor sub-region in latest-Holocene time. Such a transport asymmetry was numerically modeled for the modern Grays Harbor tidal inlet from wave and tidal flow data, as collected in the Channel Entrance sub-region between 1999 and 2002 (Osborne et al., 2003). The latest-prehistoric record of minor river sand transport to the south side of the tidal inlet area, during conditions of dominant littoral sand transport into the lower reaches of Grays Harbor, is non-intuitive. However, similar river sand bypassing mechanisms have been inferred from heavy-mineral sand source tracer studies of modern deposits in several small sand-filled estuaries in the study region (Peterson et al., 1982). Though minor in magnitude, the apparent throughput of river sand to the lowest estuarine reaches, and likely throughput across the tidal inlet to the littoral zone, denotes the onset of an important transition in river sand retention in Grays Harbor, as discussed further in Section 5.6.

Vibracore logs (2–4 m depth) of latest-Holocene deposits in Grays Harbor (Figures 5, 7, and 8) demonstrate vertical

sequences of tidal channel and tidal flat facies deposition, and/or apparent combinations of the two settings in multiple sites. Lower-intertidal channel deposit sequences, including distinctive sand and mud couplets within one meter of the deposit surface, occur in vibracores from sites G2, G8, G9, 15, G19 and G20 (n=6). Intertidal flat deposit sequences, including homogenous mud or peaty layers, occur in vibracores from sites G1, G3, G4, G13, G16 and G17 (n=6). Vibraore sites G7, G12, G14, and G18 include tidal channel sequences that transitioned up-core to tidal flat deposits (n=4). Both the similar numbers of apparent tidal channel and tidal flat depositional sequences (each n=6) and the number of apparent transitional sequences between the two different depositional settings within the vibracores (n=7) demonstrate the close intermingling of shallow tidal channel and tidal flat environments in Grays Harbor. The relations between tidal channels and tidal flats in the storage, mixing, and winnowing of sand and mud components in Grays Harbor are introduced by way of measured sedimentation rates, as discussed below in Section 5.2.

Coseismic subsidence records are widespread in marginal or peripheral tidal flat settings in Grays Harbor (Figures 5, 6, 7 and 8). Abrupt burials of upper-intertidal flat deposits, as identified from peaty mud or laminated mud >10 cm thickness, by lower-intertidal sand or sandy mud deposits totaled 14 events in 7 vibracore sites (G1, G3, G4, G5, G8, G12 and G13). Peaty mud or tidal marsh burial events were recorded in vibracores G1, G4, G12 and G18, representing coseismic subsidence (1±0.5 m) of marginal tidal flat settings in the North Bay, Inner-Harbor, and South Bay sub-regions (Figure 3). The records of coseismic subsidence in these tidal flat settings are consistent with regionally-correlated coseismic subsidence events (4–5 events each) in Grays Harbor wetland sites (Ocea2, Ellie1, and John13) (Atwater, 1997; Atwater et al., 2004; Peterson & Cruikshank, 2004). Apparent coseismic subsidence burials of upper-intertidal flat mud deposits by lower-intertidal flat sand or muddy sand units occurred as multiple events in vibracore sites G3, G5, G8 and G13 (two events each) and as a single event in vibracore sites G12, G14, and G16. The smaller number of apparent subsidence events in the tidal flat settings relative to the protected wetland settings (Ocea2, Ellie1, and John13), of equivalent subsurface depth intervals (~ 3.0 m), precludes event correlation by number/sequence relations between the two different settings.

Tidal channel responses to the cyclic sea level changes are difficult to interpret, due to complexity of both vertical and/or lateral accretion/erosion processes in the tidal channels. Nevertheless, disruptions of channel fill fining-up sequences are apparent in many vibracore sites (Figures 7 and 8). For example, an intertidal channel fill sequence in site G8 might have been initiated by a subsidence event, as recorded by submergence of an upper-intertidal flat mud. Two intertidal channel facies sequences in vibracore site G7, at 1.8 m and 2.75 m depths subsurface, might have been temporarily buried by subtidal channel sands following possible subsidence events. The AD1700 subsidence event might have disrupted an accretionary bank sequence at ~ 2.5 m depth in vibracore G15. An apparent interseismic uplift event recorded at ~1.8 m depth in vibracore G12 might have terminated tidal channel deposition at ~0.8 ka. Discontinuous coring of the larger and deeper subtidal channels in Grays Harbor (see Methods in Section 3) precludes an analysis of subtidal channel response to the short-term sea level reversals. However, the long-term vertical accretion records in some of the larger subtidal channels, such as at drill core sites D6, D8, and D15 (Figure 4) exceed the shorter recurrence intervals (500±300 years) of the neotectonic cycles (Atwater et al., 2004). Some possible relations between changes in estuary tidal prism volumes and tidal channel discharge, following tidal flat emergence/submergence events, are explored in Section 5.6 below.

5.2 Sedimentation Rate

Sedimentation rates are measured from dated intervals in tidal channel and tidal flats (Table 5) and normalized to meters per thousand years (m ka^{-1}). ^{14}C dated samples from basal sections (10-12.5 m subsurface depth) in subtidal channel deposits in drill core sites D2, D6, D8, A2, A4, D15, D17, and vibracore sites G11 and G18 yield sedimentation rates that range from 0.7 to 11.0 m ka^{-1} and average 4.2 m ka^{-1} (Table 7). Some net deposition in channel bottoms could occur from simple vertical accretion during prolonged periods of channel lateral stability. For example, drill core site D8 from the main channel in the Outer Harbor sub-region (Figures 3 and 4) recorded a long-term sedimentation rate of 0.7 m ka^{-1}. ^{14}C dating of samples in accretionary bank deposits from 5 intertidal channel settings in vibracore sites G7, G8, G15 and G19, and drill core site D15, yield sedimentation rates that range from 1.1 to 7.0 m ka^{-1} and average 3.7 m ka^{-1}. These rates are greater than corresponding rates of net sea level rise (~1.0 m ka^{-1}) in Grays Harbor during late-Holocene time (Figure 11). The high sedimentation rates in the intertidal-channel accretionary banks do not represent basin-wide sediment accumulation rates, because prolonged vertical accretion rates of intertidal deposits cannot exceed the coeval rates of net sea level rise. The lateral channel migrations in the central reaches of Grays Harbor did not promote sediment transport, but largely reworked pre-existing tidal flat deposits. The high-sedimentation rates in channel accretionary banks likely reflected high fluxes of detrital organics in the estuary, which renewed radiocarbon reservoirs in the reworked tidal channel deposits. The channel lateral migrations did effectively winnow mud from pre-existing intertidal deposits

(Figures 4, 5, 7, and 8 and Table 4), and might have enhanced horizontal asymmetry of some littoral and river sand transport. In Grays Harbor the shallow tidal channels served as sediment transport conduits rather than as sediment storage features. Substantially lower sedimentation rates are associated with tidal flat vertical accretion in vibracore sites G3, G4, G5, G12, G13 G16, and drill core sites D4, D5, and D7. The tidal flat sedimentation rates, which range from 0.7 to 2.1 m ka^{-1} and average 1.1 m ka^{-1}, are close to the estimated rate of net sea level rise (~1.0 m ka^{-1}) as shown in Figure 11. The preserved tidal flat deposits in Grays Harbor better reflect basin-wide vertical accretion, which is estimated to be ~1.0 m ka^{-1} for the entire basin fill during latest-Holocene time (Figure 11 and Table 7). Though the shallow tidal flats were associated with low sedimentation rates (~ 1.1 m ka^{-1}), their broad extents (~60% of modern estuary surface area below MHHW) (Table 1) would have substantially contributed to sediment accumulation in the shallow estuary. Though difficult to discriminate from channel lateral reworking, net vertical accretions of the subtidal settings (~40 % of modern estuarine surface area) are assumed have filled at about the rate of net sea level rise during latest-Holocene time, as was established for the preceding middle- to late-Holocene time (Peterson and Phipps, 2016).

Table 7. Deposit sedimentation rates in subtidal channels, intertidal channels and intertidal flats

Depositional setting	Core depth range (m)	Age range (ka)	Sedimentation rate (m ka^{-1})
Subtidal channels			
D2	1.0–5.5	0.0–0.9	5.0
D6	0.0–8.5	0.0–4.9	1.7
D8	0.0–3.0	0.0–4.5	0.7
A2	0.0–8.0	0.0–1.0	8.0
A4	0.0–0.9	0.0–0.9	11.0
D15	2.5–7.0	0.4–3.4	1.5
D15	7.0–13.0	3.4–6.6	1.9
D17	5.0–11.5	4.6–6.3	3.8
G11	0.0–3.5	0.0–2.7	1.3
G18	1.0–5.0	~0.3–0.9	7.0
Intertidal channels			
D15	0.0–2.5	0.0–0.4	6.2
G7	0.0–3.1	0.0–2.9	1.1
G8	0.0–2.9	0.0–1.0	2.9
G15	0.0–2.8	0.0–0.4	7.0
G16	0.0–3.4	0.0–2.7	1.2
G19	00–2.0	0.0–0.5	4.0
Intertidal flats			
D4	0.0–0.5	0.0–0.7	0.7
D5	0.0–4.0	0.0–3.6	1.1
D7	0.0–0.5	0.0–0.6	0.8
G3	0.0–3.6	0.0–4.9	0.7
G4	0.0–3.9	0.0–4.5	0.9
G5	0.0–4.0	0.0–3.2	1.2
G12	0.0–1.7	0.0–0.8	2.1
Ellie1	0.0–1.3	0.0–1.1	1.2
John13	0.0-1.9	0.0–1.4	1.3
G13	0.0–3.0	0.0–2.7	1.1

Notes: Depth intervals of identified deposit types (subtidal channel, intertidal channel, and intertidal flat) are divided by corresponding ages to yield net sedimentation rates (m ka^{-1}). See Figures 4, 5, 7 and 8 for interpreted core logs and Table 4 for deposit ages. Surface deposits are assumed to represent modern time (0 ka). The ^{14}C calibrated ages for the depth interval 1.7–3.9 m in G12 are not significantly different at 2 σ (Table 5), so that interval is not used in this analysis. Tidal marsh sedimentation rates following the last coseismic subsidence event (AD1700) could have been influenced by early- historic increases in river sediment supply (Barrick, 1976). They are not used for this comparative analysis.

Assuming a basin-wide net sedimentation rate of ~1.0 m per 1,000 years, annual net rates of sediment accumulation can be calculated for the sediment components in the sub-regions of Grays Harbor (Table 6**)**. Taking the total basin accumulation rate for all sediment components (232 x 10^6 m^3 ka^{-1}) and dividing by 1,000 years yields an annual rate of 0.23 x 10^6 m^3 yr^{-1}. This value is nearly one half of the longer-term net accumulation rate (0.4 x 10^6 m^3 yr^{-1}) estimated for the middle- to late-Holocene period, corresponding to the uppermost 10 m depth interval in Grays Harbor (Peterson & Phipps, 2016). The net accumulation rate in latest-Holocene time (3-0 ka), or the uppermost ~3.0 m depth interval in Grays Harbor, decreased in magnitude from earlier accumulation rates following decreased rates of sea level rise in latest-Holocene time (Figure 11). The lower rates of sea level rise reduced the rate of increasing accommodation space in Grays Harbor (Peterson & Phipps, 2016), thereby further limiting sediment accumulation rates during latest-Holocene time. The mechanisms that limited sediment accumulation rates in the Grays Harbor basin under the low rates of sea level rise in latest-Holocene time are discussed below in Sections 5.5 and 5.6.

5.5 Tidal Flat Deposit Resuspension by Wind Waves in Grays Harbor

The broad intertidal areas in the central reaches of Grays Harbor (Figure 2) are generally limited to lower-intertidal elevations (Table 3). Neither mud flats nor tidal marshes presently extend beyond tidal creek tributary valleys or eastern spit shorelines (Figure 2), which are protected from wind-wave erosion. What critical wind-wave fetch distances prohibit tidal marsh progradation in Grays Harbor? Maximum fetch distances of onshore (westerly) wind- waves in Grays Harbor are 10±5 km in length (Figure 13). The longest fetch distance (~15 km) extends from the harbor mouth to the Inner Harbor sub-region. However, short northeast and southeast fetch distances (≤ 5 km) to lee shorelines in the eastern Inner Harbor sub-region are restricted by the narrowing river valley morphology. The protected shorelines in the Inner-Harbor sub-region show recent accretion of channel overbank and/or supratidal marsh deposits, such as at sites A1-4 (Phipps et al., 2015). Substantial fetch distances (10–14 km) extend into the Outer Harbor sub-region where northwest and southeast lee shorelines show stability or recent erosion. Small gravelly-sand beach berms are presently developed along some of those wind-wave-impacted shorelines. Modest maximum fetch distances of 5–10 km and 3–8 km, respectively, occur in the North Bay and South Bay sub-regions, where significant tidal marsh progradation (>0.5 km width) is limited to the shorter fetch distances (< 5 km) in the southern part of the South Bay sub-region.

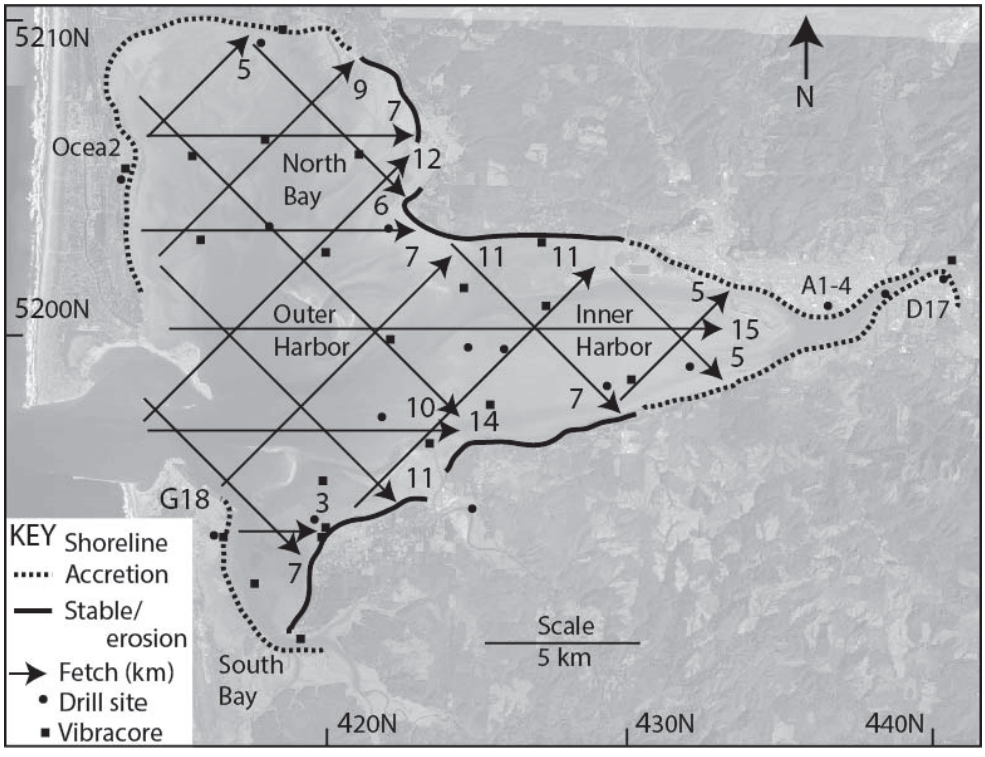

Figure 13. Map of shoreline conditions and corresponding wind wave fetch distances in Grays Harbor

Maximum wind-wave fetch distances (arrows) in Grays Harbor are shown for wind-wave propagations in three

representative directions, east, northeast and southeast, respectively, from corresponding wind directions 270°, 225° and 315° N. Historic shoreline conditions of accretion or stable/erosional, respectively, correspond to shorter (≤ 5 km) and longer (≥ 10 km) maximum fetch distances. Representative fetch distances over the Grays Harbor tidal flats, for the range of expected onshore wind directions (225-315° N), generally range from 2.5 km to 10 km in distance.

In addition to the limited tidal marsh progradation in exposed peripheral shorelines, wind-waves also play important roles in re-suspending sediments in the broad interior tidal flat settings (-1.5-0 m MTL) in Grays Harbor. To what extent might wind-waves control the elevations or accommodation space in the lower-intertidal flat settings? To address that question wind forcing data are combined with fetch distances and mesotidal submergence depths to predict the erosional capabilities of maximum wind-wave conditions in Grays Harbor. Local wind conditions in Grays Harbor are well established from a continuously operated anemometer station at the harbor mouth (Station WPTW1 in Figure 2**)**. Maximum westerly wind velocities (<5% probability for averaged 0.1 hr durations) reach 10 to 14 m s^{-1} during winter months (NDBC, 2017). For the purposes of this article we compile high velocity wind events with ≥ 10 m s^{-1} average velocities for durations ≥3.0 hour (≥ 0.25 tidal cycle) that occurred in Grays Harbor during the year 2012 (Table 9). Monthly wind speed averages for the year 2012 are representative of monthly averages for the preceding years 2008–2011, which together represent the extent of historic continuous wind data recorded at Station WPTW1.

Table 9. Events of sustained high velocity winds in Grays Harbor during the year 2012.

mo/dy/hr	Duration (hr)	Bearing (N°)	Velocity (ms^{-1})	mo/dy/yr	Duration (hr)	Bearing (N°)	Velocity (ms^{-1})
01/02/22	5	216	14	03/29/05	5	188	12
01/04/12	9	190	11	03/31/10	5	92	13
01/05/09	3	246	10	04/01/04	9	287	13
01/10/07	5	336	11	04/13/22	4	336	11
01/14/17	11	290	12	04/30/17	10	273	11
01/17/10	3	261	10	05/03/22	6	309	11
01/18/11	9	101	12	05/08/20	11	336	12
01/19/17	4	94	10	05/09/21	7	324	10
01/21/09	3	275	13	05/10/24	5	342	10
01/21/14	8	274	11	05/12/22	6	344	11
01/22/21	5	241	12	05/13/20	6	340	11
01/25/00	9	231	12	05/15/22	9	326	11
01/26/05	13	286	12	06/05/02	13	311	10
02/01/12	3	320	12	10/12/19	6	190	11
02/07/06	4	100	11	10/14/18	6	192	11
02/18/02	14	269	14	11/12/03	5	190	11
02/21/20	5	255	10	11/21/18	7	270	12
02/22/08	22	295	11	12/01/10	11	211	12
02/25/06	9	302	12	12/02/20	9	240	11
02/29/13	8	255	12	12/03/08	4	233	11
03/05/12	26	303	13	12/05/02	9	268	12
03/15/06	9	192	12	12/07/18	6	312	12
03/20/07	8	242	11	12/17/03	21	274	14
03/24/14	6	98	11	12/27/00	10	295	11

Notes: Wind forcing events for sustained very-high winds, with averaged means ≥ 10 m s^{-1} and durations ≥ 3.0 hour (≥ 0.25 tidal cycle) for the year 2012 from Station WPTW1, Westport, Grays Harbor, Washington. Wind event parameters include durations (hours), mean velocities (ms^{-1}) and mean bearings (°N). Data are compiled from NDBC (2017).

The year 2012 totaled 48 sustained (≥3.0 hour) high velocity (≥ 10 m s^{-1}) wind events. The mean and standard deviation of averaged velocities for the westerly wind events (n=44) are 11±1 1σ m s^{-1}. The mean and standard deviation of averaged wind bearings for the n=44 westerly wind events are 267±54 1σ ° N. Though of low frequency, several sustained wind events (n=4 events) of high velocity easterly winds (bearings 92–101° N) did

occur in Grays Harbor in 2012. Such infrequent easterly wind events would have forced wind-wave propagation to the west, thus accounting for the limited progradation (< 0.5 km) of tidal marsh deposits along the eastern side of the North Spit and the northernmost eastern shores of the South Spit (Figure 2) (Peterson et al., 2010).

For the purposes of this article, high-velocity wind speeds of 10 m s^{-1} and 12 m s^{-1} are used to estimate maximum sustained wind-wave heights and periods in the shallow tidal flats of Gays Harbor. A range of wind-wave forcing fetch distances, 2.5 km, 5.0 km, and 10.0 km are taken from Figure 13. A range of water depths, 0.5 m, 1.0 m, 1.5 m, 2.0 m, and 2.5 m over the intertidal flats (MLLW-MHHW) are assumed for the mesotidal ranges of ≤ 3.0 m in Grays Harbor. Wind-wave heights and periods are calculated (Table 10) using the online application SPMWave.html, for fetch and depth limited wave calculations (USGS, 2017a). Maximum bottom orbital velocities are calculated (Table 11) for a range of sustained maximum wind-wave conditions and water depths (1.0–4.0 m) using the online application RunWaveCalcs.html, for linear wave calculations (USGS, 2017b).

Table 10. Predicted maximum sustained wind-wave heights and periods.

Wind Speed (m s^{-1})	Fetch Distance (km)	Water depth (0.5 m) Wave ht (m)/ period (s)	Water depth (1.0 m) Wave ht (m)/ period (s)	Water depth (1.5 m) Wave ht (m)/ period (s)	Water depth (2.0 m) Wave ht (m)/ period (s)	Water depth (2.5 m) Wave ht (m)/ period (s)
10.0	2.5	0.16/1.54	0.23/1.67	0.26/1.73	0.27/1.76	0.28/1.78
	5.0	0.17/1.74	0.26/1.95	0.32/2.05	0.34/2.10	0.36/1.15
	10.0	0.17/1.90	0.29/2.21	0.36/2.37	0.42/2.46	0.46/2.53
12.0	2.5	0.18/1.65	0.27/1.79	0.31/1.86	0.33/1.90	0.35/1.92
	5.0	0.19/1.86	0.31/2.09	0.37/2.20	0.42/2.27	0.44/2.31
	10.0	0.20/2.03	0.32/2.37	0.42/2.54	0.49/2.65	0.54/2.73

Notes: Wind-wave height (m) and period (s) are predicted on the bases of maximum averaged wind speeds (10 and 12 m s^{-1}), fetch distances (2.5, 5.0 and 10 km), and water depths (0.5 m, 1.0 m, 2.0 m and 2.5 m), using SPMWave.html calculator (USGS, 2017a). Wave development is not duration limited for the infrequent sustained periods (≥ 3.0 hr) of very-high velocity winds (Table 10) over the representative fetch distances (2.5–10 km) in Grays Harbor (Figure 13).

Table 11. Estimated near–bottom orbital velocities from predicted wind–waves and water depths.

Wave height (m)	Wave period (s)	Water depth (m)	Orbital velocity (m s-1)
0.2	2.0	1.0	0.20
		2.0	0.08
		3.0.	0.03
		4.0	0.01
0.3	2.2	1.0	0.34
		2.0	0.15
		3.0	0.07
		4.0	0.03
0.4	2.7	1.0	0.51
		2.0	0.28
		3.0	0.17
		4.0	0.10
0.5	2.8	1.0	0.65
		2.0	0.36
		3.0	0.22
		4.0	0.14

Notes: Wind–wave orbital velocity (m s^{-1}) is estimated for predicted wave height (m), wave period (s), and water depth (Table 11), using RunWaveCalcs.html calculator (USGS, 2017b). Orbital velocities > 0.2 m s^{-1} are above the threshold for the erosion of fine sand (Table 4) in the shallow tidal flats of Grays Harbor.

Maximum wind-wave development during high-tides (~2.0 m submergence) and long fetch distances (~10 km) in

Grays Harbor (Figure 13) could have reached heights of ~0.5 m and periods of ~2.7 seconds (Table 10). Wind-waves of lower heights (0.27–3.3 m) would have been produced by the same conditions over shorter fetch distances (2.5–5.0 km). Wave heights of only ≤0.2 m would have predominated during the lower tidal submergences of ~0.5 m water depth. Bottom wave orbital velocities are calculated for the range of predicted wave heights (0.2–0.5 m) and potential water depths (1.0–4.0 m) (Table 11). Orbital velocities of ≥ 0.2 m s^{-1} are needed to re-suspend fine sand (Table 4) off the bottom of sandy tidal flats in Grays Harbor. The smallest wave heights (~0.2 m) could have re-suspended sand down to water depths of ~1.0 m. The largest wave heights (0.5 m) could have re-suspended sand down to water depths of ~3.0 m. This depth range of wind-wave re-suspension of fine sand in submerged tidal flats accounts for the reported preponderance of shallow lower-intertidal flat depths within reach of modest fetch distances (5–15 km) in the lower reaches of Grays Harbor. Drift currents from tidal flow and/or wind shear flow likely serve to disperse the tidal flat sediments during repeated wind-wave re-suspension cycles.

The upper vertical accretion elevations (-1.5 to 0 m MTL) of interior tidal flats in Grays Harbor (Table 3) are limited by wind-wave truncation during sustained high-velocity wind forcing events (Tables 10 and 11). In effect, wind-wave truncation determines available accommodation space, at a given sea level, for sediment deposition and retention in the broad tidal flats of Grays Harbor. The tidal flat depths for corresponding surface areas also control the tidal prism volumes in Grays Harbor (Table 1). For example, the modern tidal prism volume between MLLW and Mean tidal level (2.5 x 10^8 m^3) is only 41 % of the tidal prism volume between MLLW and MHHW (6.1 x 10^8 m^3) (Table 1). An equivalent of 1.5 m of tidal flat submergence yields 60 % greater tidal discharge, which drives tidal flow and peak transport velocities in the Grays Harbor tidal channels, as diagramed below in Section 5.6.

5.6 Models of Interactive Accommodation Space Controls

In this section, the interactions between tidal channel transport, tidal flat accretion, and tidal flat erosion are explored in terms of potential accommodation space controls in the broad shallow tidal settings in Grays Harbor. Relatively rapid submergence of the ancestral Chehalis River valley in early-Holocene time (Peterson and Phipps, 2016) resulted in a central basin with small tidal prism:subtidal prism ratios and weak currents in broad channel bottoms (Figure 14A). By late-Holocene time the low rates of net sea level rise (Figure 11) permitted sediment infilling of the central basin and the development of constricted channels (Figure 2). High tidal prism:subtidal prism ratios, such as the modern maximum tidal prism ($6.6x10^8$ m^3) to subtidal prism ($3.9x10^8$ m^3) ratio of 1.7 (Table 1), produced strong reversing tidal currents in the constricted channels (Figure 14B). Slightly-asymmetric channelized tidal flows provided the transport energies needed to import both littoral sand and river sand into the central reaches of Grays Harbor. Tidal current transport of sand and mud onto the tidal flats promoted vertical accretion, but the vertical accretion did not reach high tidal water levels (Table 3). Wind-wave resuspension of tidal flat deposits provided the energy to winnow mud from the tidal flat deposits (Tables 10 and 11), permitting fluvial-ebb tidal currents to export mud and possibly some fine river sand out of the estuary (Figure 14C). If high tide 'slack-water' deposition had continued to infill the lower-intertidal flats to supratidal floodplain levels then the total-basin tidal prism would have diminished, as well as the corresponding tidal channel discharge. Diminished flood tidal discharge would have 1) decreased the import of littoral sand into the estuary and 2) likely enhanced the export of river sediments out of the partially- to well-mixed estuary. Tidal flat elevations and associated tidal prism volumes controlled tidal channel discharge velocities and flood tidal to riverine-ebb flow ratios in Grays Harbor, thus influencing littoral sand import and river sediment export in Grays Harbor. The wind-wave energy not only limited tidal flat elevations but also indirectly influenced tidal channel discharge and channelized sediment transport in Grays Harbor. These interacting processes of sediment supply and transport energies also adjusted to relative sea level changes from both eustatic and neotectonic processes, as discussed below.

Part A. A conceptual total-basin model for a middle-Holocene central basin, including a large subtidal prism and corresponding low velocity flows in broad channel bottoms. Part B. A conceptual total-basin model of a filled central basin by late-Holocene time, leading to shallow tidal flats, constricted tidal channels, and corresponding high velocity flows in the narrow tidal channels. Part C. Equilibrium lower-intertidal flat elevations relative to wind-wave orbital current erosion/truncation (deepening) and slack water deposition and vertical accretion (shallowing). Part D. Interseismic uplift causing tidal flat emergence, decreasing tidal prism volume and decreasing intertidal channel discharge/flow velocities. Part E. Coseismic subsidence causing tidal flat submergence, increasing tidal prism volume and increasing tidal channel discharge/flow velocities.

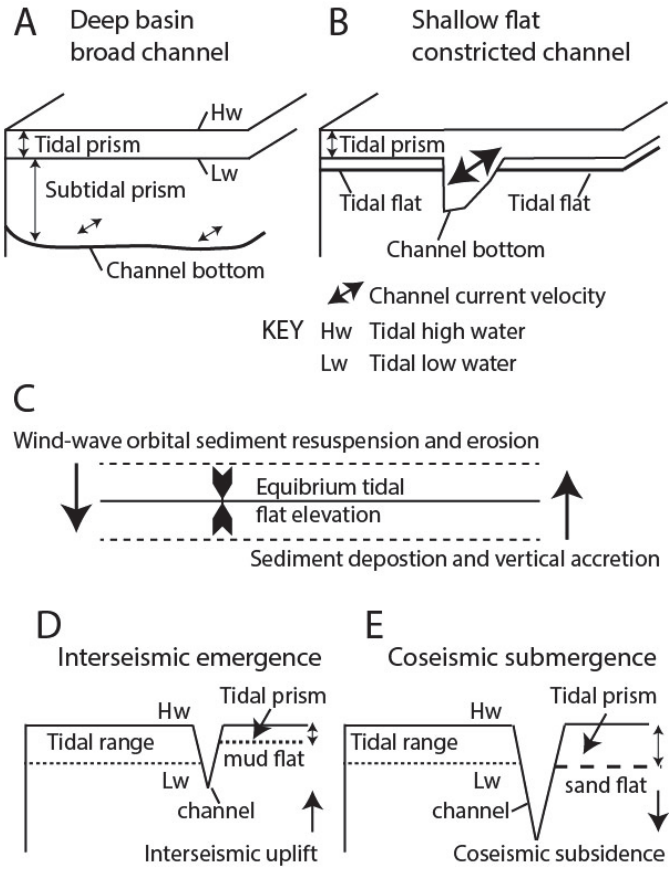

Figure 14. Diagrams of depositional accommodation space controls in the Grays Harbor basin

Neotectonic cycles of interseismic uplift and coseismic subsidence, respectively, reversed tidal flat emergence and submergence on multi-century time scales in Grays Harbor (Figures 14D and 14E). These short-term sea level changes were superimposed on a longer-term and progressive eustatic sea level rise (~1.0 m ka^{-1}) (Figure 11) in latest-Holocene time. The reversing neotectonic sea level changes did not contribute to the long-term curves of net sea level rise and net sediment deposition in Grays Harbor. However, the neotectonic cycles of tidal flat emergence and submergence did have 1) direct impacts on tidal flat deposit compositions and 2) likely impacts on total-basin tidal prism volumes and associated tidal channel discharges, as based on disrupted intertidal channel facies sequences (Figures 5, 7 and 8). The magnitudes and durations of abrupt coseismic submergence (1±0.5 m paleo-tidal level change for 100–200 years) in the CRLC system (Peterson et al., 2010; Peterson and Vanderburgh, 2018) are not dissimilar from predictions of near future sea level rise (DeConto & Pollard, 2016; Mengel et al., 2016). In this regard, the latest-Holocene depositional records in Grays Harbor provide insights to tidal flat and tidal channel responses to potential rapid sea level rise in other estuaries with similar depositional settings to those in Grays Harbor. Modest rapid submergence (1–2 m) of intertidal flats in Grays Harbor resulted in increased transport and net deposition of littoral sand on the broad interior intertidal flats. Slow tidal flat emergence, from interseismic uplift and sedimentation, lead to lower-energy deposition of mud and peaty-mud deposits, and possibly to enhanced export of some river sand out of the estuary.

A late-Holocene sediment budget is shown for Grays Harbor in Figure 15A. The sediment budget is based on measured volume accretion rates (x 10^6 m^3 ka^{-1}) from Table 6, which are divided by 10^3 yr to yield annual accumulation rates (x 10^3 m^3 yr^{-1}). For example, the annual rate of littoral sand import into Grays Harbor during latest-Holocene time is estimated to be 117 x 10^3 m^3 yr^{-1}. This compares to about twice the annual rate of river sand annual accumulation (60 x 10^3 m^3 yr^{-1}) in the Grays Harbor estuary during latest-Holocene time. A small but important asymmetry of littoral sand import and possible river sand export is shown for the main-channel in the lowermost reaches of Grays Harbor (Figure 15A). The most seaward rate of river sand transport (3 x 10^3 m^3 y^{r-1}) is a minimum value, as it is based on the net accumulation rate of river sand in the lower estuarine reaches (Table 6). The annual rate of river sand that is bypassed through the estuary to the littoral zone could be substantially greater, as it might be masked by a large reversing flux of littoral sand in the tidal inlet area. An annual rate of river

sand throughput could reach as much as 30 x 10^3 m^3 yr^{-1}, if the total river sand accumulation rate (60 x 10^3 m^3 yr^{-1}) (Table 6) is subtracted from the historic river sand supply rate (90 x 10^3 m^3 yr^{-1}) (Karlin, 1980; Peterson and Phipps, 2016). Similarly, a possible annual rate of river mud exported out of Grays Harbor (305 x 10^3 m^3 yr^{-1}) can be estimated from the subtraction of the total mud accumulation rate (55 x 10^3 m^3 yr^{-1}) (Table 6) from the estimated historic rate of river mud supply (360 x 10^3 m^3 yr^{-1}) (Karlin, 1980; Peterson & Phipps, 2016). It is not known to what extent the historic river sediment supply rates might have increased relative to pre-historic rates due to logging and agriculture impacts in the tributary drainages (Barrick, 1976). The possible bypassing of river sand through the Grays Harbor estuary to the littoral zone in latest-Holocene time addresses a deficit in river sand accumulation rates during late-Holocene time that was reported by Peterson & Phipps (2016). It that article the deficit was attributed to river sand accumulation in the tributary valleys located upriver of the estuary. In this article, we attribute, at least part of, the apparent deficit in the river sand accumulation rates in late-Holocene time in Grays Harbor to an onset of river sand bypassing though the estuary to the littoral zone.

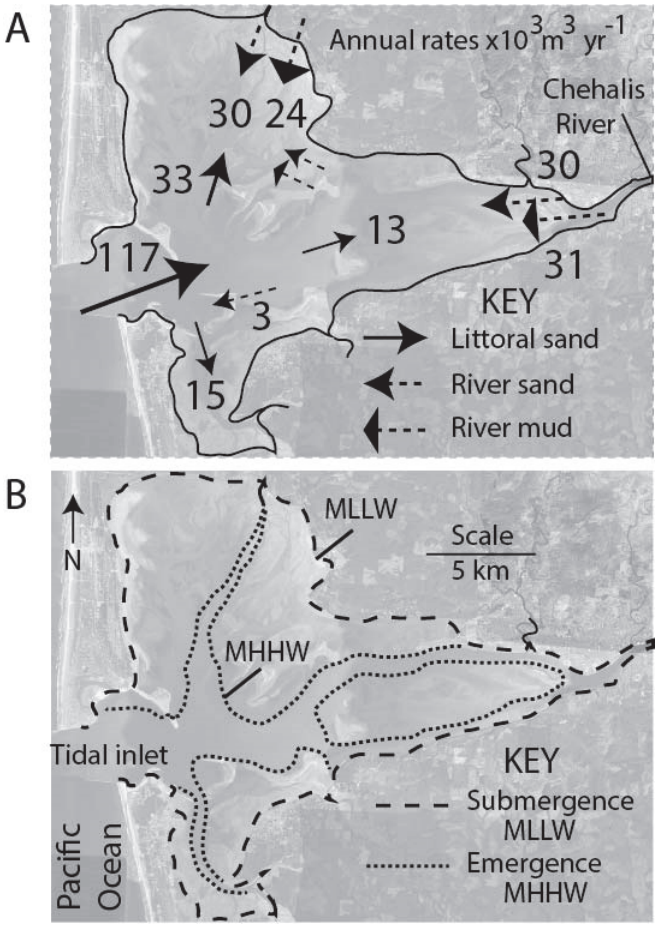

Figure 15. Diagrams of latest-Holocene sediment budgets and possible future shoreline in Grays Harbor

Part A. Map of latest-Holocene sediment budgets in Grays Harbor, based on measured long-term sediment component accumulation rates divided by 10^3 yr to yield average annual accumulation rates (x 10^3 m^3 yr^{-1}). Annual input rates (x 10^3 m^3 yr^{-1}) associated with directional arrows show the net annual volumes that pass through corresponding conduits to reach sub-regions (Figure 3) of estimated net accumulations (Table 6). Sediment components include littoral sand (bold line with arrows), river sand and river mud (dashed lines with arrows). Part B. Map of possible endmember conditions of future tidal flats in Grays Harbor, including 1) submergence of intertidal flats to subtidal levels and retreat of MLLW shorelines (dashed lines) or 2) emergence of intertidal flats to supratidal elevations and progradation of the MHHW shorelines (dotted lines).

Stabilization and/or deepening of the Chehalis River, and the North and South Channels in the Inner Harbor sub-region has been underway since early historic time (1903) (USACE, 1903). Construction of the south jetty (1898–1902) and the north jetty (1908–1916) stabilized the channel entrance, but caused shallowing and shoaling in the

Outer Harbor sub-region (Kaminsky et al., 2010). Between 1894 and 1927 channel dredging and dredge spoil disposal in Grays Harbor averaged 0.6 x 10^6 m^3 yr^{-1}. Deepening and maintenance of the shipping channel (Figure 2) has been performed by pipeline and hopper dredge, with dredge spoils disposal located largely in the Channel Entrance sub-region. For the years 1966 to 1975, a representative mid-historic time interval, channel dredging and dredge spoils disposal in Grays Harbor ranged from 1.0 x 10^6 m^3 yr^{-1} to 1.6 x 10^6 m^3 yr^{-1} (Barrick, 1976). The annual dredging and dredge spoils disposal in Grays Harbor for the year 2017 is reported to be 6 x 10^5 m^3 (USACE, 2017). Those volumes substantially exceed the measured latest-Holocene annual accumulation rates of all sediment components in the estuary (0.23 x 10^6 m^3 yr^{-1}) (Figure 15A). The natural (prehistoric) sediment budget in Grays Harbor (Table 6 and Figure 15) has been substantially impacted by anthropogenic activities in the estuarine reaches and harbor mouth areas.

As discussed above, intertidal flat elevations in Grays Harbor (Table 3) have been buffered from small changes in sea levels and sediment supply during latest-Holocene time (Figure 14). However, several potential factors including future diking/filling activities, global sea level rise, and/or the spread of invasive stabilizing vegetation, could overcome the balance of accommodation space controls that have operated in Grays Harbor for the last several thousand years. For example, a mean lower low water (MLLW) shoreline could retreat to the present uppermost intertidal shorelines (Figure 15A), following 2–3 m of submergence from future sea level rise (Kopp et al., 2014; Mengel et al., 2016; DeConto & Pollard, 2016). Such submergence would largely eliminate lower-intertidal flat habit for migratory bird feeding, commercial shellfish, and other ecosystem functions. In contrast, a mean higher high water (MHHW) shoreline could prograde out to the deepest modern subtidal channels (Figure 15B) following infilling of intertidal flats. Suh infilling could arise from decreased wind-wave energy due to reduced distances of wind-wave fetch (Figure 13). Wind-wave fetch distances could be shortened by 1) shoaling from diking/filling or misplaced disposal of dredge spoils (Osborne et al, 2002 Osborne et al., 2003) and 2) by the spread of invasive stabilizing vegetation *Spartina* (WSDA, 2016). Uncertainties about future tidal flat conditions in Grays Harbor underscore uncertainties about the potential magnitudes of different anthropogenic impacts to the pre-existing accommodation space balances in the large shallow mesotidal estuary.

6. Conclusions

Grays Harbor provides ideal conditions to investigate the interactions between accommodation space controls of tidal channel and tidal flat deposition under variable conditions of sea level change in a shallow mesotidal wave-dominated estuary. Sediment samples from drill cores and vibracores (3-4 m depth subsurface) were analyzed for tidal flat and tidal channel facies discrimination, sediment grain size distributions, littoral versus river sand source, and basal core deposit ^{14}C age. Sediment sample analyses were averaged within five sectors or sub-regions, and then totaled to estimate estuary basin accumulation rates, as normalized to a mean sedimentation rate of ~1.0 m per 1.0 ka. During latest-Holocene time (3–0 ka) the littoral sand accumulation rates in Grays Harbor were double those of river sand and river mud accumulation rates. The effective transport of littoral sand into the estuary is attributed to asymmetric channel bottom flow and sand migration over broad tidal flats. The export of river mud out of the estuary is attributed to net ebb surface flow and resuspension of the mud fraction in shallow tidal flat deposits by wind-wave winnowing and lateral channel migration. The reworking of pre-existing deposits by lateral channel migration dominates the latest-Holocene depositional record but channel migration is not thought to substantially influence basin-wide sediment accumulation rates. Total sediment accumulation rates are directly tied to the rate of relative sea level rise, or increasing accommodation space in the estuary. Intertidal accommodation space in the broad tidal flats is controlled by wind wave truncation of upper-intertidal flat deposits. The unfilled intertidal space, resulting from wind-wave erosion, maintains a large tidal prism, which drives strong tidal flows in the constricted tidal channels. The strong tidal channel flows transport littoral sand into the estuary and possibly some river sand out of the estuary. However, the import of littoral sand into Grays Harbor is ultimately linked to the selective export of river mud out of the estuary, which otherwise would have over-filled the existing basin accommodation space. The delicate balance between modest net sea level rise, net sediment import/export, and basin-wide sedimentation rate maintained the broad intertidal flat settings in Grays Harbor throughout latest-Holocene time. The intertidal flats generally survived small sea level reversals from neotectonic uplift/subsidence cycles. However, the natural balance between sea level rise, sedimentation rate, and tidal flat levels in Grays Harbor could be dramatically altered by 1) rapid sustained rise of eustatic sea level, following ongoing global warming, 2) reduction of wind-wave fetch distance and associated wind-wave erosion of tidal flats, due to tidal flat diking/filling, and/or 3) uncontrolled spread of non-native invasive sediment stabilizing sea grass (*Spartina*). The apparent susceptibility of the balanced sediment dynamics in Grays Harbor to potential future anthropogenic impacts serve as a warning for other similarly balanced estuarine depositional systems and associated intertidal ecosystems, under threat from potential future anthropogenic impacts.

Acknowledgements

James B. Phipps and Kenneth F. Scheidegger provided these authors with early introductions to the modern sedimentology processes in Grays Harbor. Brian Atwater provided wetland site locations with representative coseismic subsidence records. David Hollingswoth operated the oyster dredge Maisha that was used for shallow tidal deposit vibracoring in Grays Harbor. Dave Qualman, Oscar Sorenson, and Heather Bragg assisted with vibracoring and core logging. Kenneth Cruikshank assisted with NDBC anemometer station data analysis and wind wave height and orbital velocity calculations. Support for vibracoring in Grays Harbor was provided by the U.S. Geological Survey, Coastal and Marine Geology Program, under the South West Washington Coastal Erosion Project, Co-op #1434-HQ-96-AG-01612 from 1996-2001. Field logistical support was provided by Grays Harbor College, Washington, USA. Additional support for radiocarbon dating was provided by Medicine Hat College, Medicine Hat, Alberta, Canada.

References

Allen, G. P., & Posamentier, H. W. (1993). Sequence stratigraphy and facies models of an incised valley fill: the Gironde estuary, France. *Journal of Sedimentary Petrology, 63*, 378-391.

Atwater, B. F. (1992). Geologic evidence for earthquakes during the past 2000 years along the Copalis River, southern coastal Washington. Radiocarbon dates in Appendix as Supplement. *Journal of Geophysical Research, 97*, 1901-1919. https://doi.org/10.1029/91JB02346

Atwater, B. F. (1997). Coastal evidence for great earthquakes in Western Washington. *U.S. Geological Survey Professional Paper 1560,* pp. 77-90.

Atwater, B. F., Tuttle, M. P., Schweig, E. S., Rubin, C. M., Yamaguchi, D. K., & Hemphill-Haley, E. (2004). Earthquake recurrence, inferred from paleoseismology, in Gillespie, A.R., Porter, S.C., and Atwater, B. F., editors, The Quaternary Period in the United States: Amsterdam, Elsevier, p. 331-350.

Baker, D., Peterson, C., Hemphill-Haley, E., & Twichel, D. (2010). Holocene sedimentation in the Columbia River Estuary. *Marine Geology, 273*, 83-95. https://doi.org/10.1016/j.margeo.2010.02.005

Barnett, E. T. (1997). Potential for coastal flooding due to coseismic subsidence in the central Cascadia margin. M.S. Thesis, Portland State University, 144 p.

Barrick, R. C. (1976). Hydrodynamics of Grays Harbor estuary, Washington. Appendix A: In Knott, N.P., and Barrick, R. C., (eds). Maintenance dredging and the environment of Grays Harbor, Washington. U.S. Army Corps of Engineers, Seattle District., 16 p.

Byrnes, M., R., & Li, F. (1998). Regional analysis of sediment transport and dredged material dispersal patters, Columbia River mouth, Washington/Oregon. Final Report to US Army Corps of Engineers Waterways Experiment Station. Applied Coastal Research and Engineering, Inc. Mashpee, MA. 53, pp.

Calib7.10 (2017). Radiocarbon Calibration Program. CALIB REV7.1.0. http://calib.org/calib/calib.html. Accessed November 17, 2017.

Clifton, H. E., & Phillips, R. L. (1980). Lateral trends and vertical sequences in estuarine sediments, Willapa Bay, Washington. In M. E., Field, (Ed.), *Quaternary depositional environments of the Pacific coast*. Pacific Coast Paleogeography Symposium 4, Society for Economic Paleontologists Mineralogists Pacific Section. pp. 55-71.

Dalrymple, R. W., Boyd, R., & Zaitlin, B. A. (1994). Incised–valley systems: Origins and Sedimentary Sequences. SEPM Society for Sedimentary Geology. Special publication No. 51.

Dalrymple, R. W., Zaitlin, B. A., & Boyd, R. (1992). Estuarine facies models: conceptual basis and stratigraphic implications. *Journal of Sedimentary Petrology, 62*, 1130-1146. https://doi.org/10.1306/D4267A69-2B26-11D7-8648000102C1865D

DeConto, R. M., & Pollard, D. (2016). Contribution of Antarctica to past and future sea-level rise. *Nature, 531*, 591-597. https://doi.org/10.1038/nature17145

Google Earth (2018). *Google Earth.* Retrieved February 15, 2018, from https://www.google.com/earth/

Kaminsky, G. M., Ruggiero, Buijsman, M. C., McCandless, D., & Gelfenbaum, G. (2010). Historical evolution of the Columbia River littoral cell. Marine Geology*, 273*, 96-126. https://doi.org/10.1016/j.margeo.2010.02.006

Kopp, R. E., Horton, R. M., Little, C. M., Mitrovica, J. X., Oppenheimer, M., Rasmussen, D. J., Strauss, B. H., & Tebaldi, C. (2014). Probabilistic 21st and 22nd century sea-level projections at a global network of tide-gauge

sites. *Earth's Future, 2*, 383-406. https://doi.org/10.1002/2014EF000239

Mengel, M., Levermann, A., Frieler, K., Robinson, A., Marzeion, B., & Winkelmann, R. (2016). Future sea level rise constrained by observations and long-term commitment. *Proceedings of the National Academy of Sciences, 113*, 2597-2602. https://doi.org/10.1073/pnas.1500515113

Milliman, J. D. (1963). Recent marine sediments in Grays Harbor, Washington. M.S. Thesis, University of Washington, Department of Oceanorgraphy, Seattle, Washington 169 p.

NDBC. (2017). National Data Buoy Center, National Oceanic and Atmospheric Administration. Station WPTW1, Westport, Washington. Climatic Summary Plots for wind speed and Historic Data Download. http://www.ndbc.noaa. *Accessed November, 27*, 2017.

Osborne, P. D., Davies, M. H., & Cialone, M. A. (2003). Sediment transport paths at Grays Harbor, Washington. Proceeding Coastal Sediments '03–5th International Symposium on Coastal Engineering and Science of Coastal Sediment Processes, Clearwater, Beach, FLA. p.1–14.

Osborne, P. D., Hericks, D. B., Kraus, N. C., & Parry, R. M. (2002). Wide-area measurements of sediment transport at a large inlet, Grays Harbor, Washigton. Proceedings 28th International Conference on Coastal Engineering. World Scientific, Cardiff, Wales, pp. 3053-3064.

Peterson, C. D., & Cruikshank, K. M. (2014). Quaternary tectonic deformation, Holocene paleoseismicity, and modern strain in the unusually-wide coupled zone of the central Cascadia margin, Washington and Oregon, USA and British Columbia, Canada. *Journal of Geography and Geology*, *6*, 1-33. https://doi.org/10.5539/jgg.v6n2p1

Peterson, C. D., & Phipps, J. B. (1992). Holocene sedimentary framework of Grays Harbor basin, Washington, USA. Quaternary Coastal Systems of the United States, Marine and Lacustrine Systems: SEPM Society for Sedimentary Research, Special Publication No. 48, 273-285 pp.

Peterson, C. D., & Phipps, J. B. (2016). Accommodation space controls on incised-valley sediment accumulation rates during the Holocene marine transgression (0–11 ka) in Grays Harbor, a large meso-tidal estuary, Washington, USA. *Marine Geology, 380*, 1-16. https://doi.org/10.1016/j.margeo.2016.06.012

Peterson, C. D., & Scheidegger, K. F. (1984). Holocene depositional evolution in a small active- margin estuary of the northwestern United States. *Marine Geology 59,* 51-83. https://doi.org/10.1016/0025-3227(84)90088-4

Peterson, C. D., & Vanderburgh, S. (2018). Tidal flat depositional response to neotectonic cyclic uplift and subsidence (1–2 m) as superimposed on latest-Holocene net sea level rise (1.0 m/ka) in a large shallow mesotidal wave-dominated estuary, Willapa Bay, Washington, USA. *Journal of Geography and Geology, 10*, 109-139. http://dx.doi.org/10.5539/jgg.v10n1p109

Peterson, C. D., Doyle, D. L., & Barnett, E. T. (2000). Coastal flooding and beach retreat from coseismic subsidence in the central Cascadia margin, USA. *Environmental and Engineering Geology, 6*, 255-269. https://doi.org/10.2113/gseegeosci.6.3.255

Peterson, C. D., Scheidegger, K. F., & Komar, P. D. (1982). Sand dispersal patterns in an active- margin estuary of the northwestern United States as indicated by sand composition, texture and bedforms. *Marine Geology, 50*, 77-95. https://doi.org/10.1016/0025-3227(82)90062-7

Peterson, C. D., Scheidegger, K. F., Niem, W., & Komar, P. D. (1984). Sediment composition and hydrography in six high-gradient estuaries of the northwestern United States. *Journal of Sedimentary Petrology, 54*, 86-97.

Peterson, C. D., Twichell, D. C., Roberts, M. C., Vanderburgh, S., & Hostetler, S. W. (2016). Accommodation space in a high-wave-energy inner-shelf during the Holocene marine transgression: Correlation of onshore and offshore inner-shelf deposits (0–12 ka) in the Columbia River littoral cell system, Washington and Oregon, USA. *Marine Geology, 379*, 140-156. https://doi.org/10.1016/j.margeo.2016.05.007

Peterson, C. D., Vanderburgh, S., & Roberts, M. (2014). Late Holocene Geomorphology of the Columbia River Estuary, Oregon and Washington, USA. *Journal of Geography and Geology, 6*, 1-27. https://doi.org/10.5539/jgg.v6n2p1

Peterson, C. D., Vanderburgh, S., Roberts M. C., Jol, H. M., Phipps, J. P., & Twichell, D. C. (2010). Composition, age, and depositional rates of Holocene shoreface deposits under barriers and beach plains of the Columbia River littoral cell, USA. *Marine Geology, 273*, 62-82. https://doi.org/10.1016/j.margeo.2010.02.004

Phipps, J. B., Gage, B., & Caryl, J. (1976). Grain size analyses of some Grays Harbor sediment samples, Appendix

C. In Knott, N.P., and Barrick, R.C., (eds) Maintenance dredging and the environment of Grays Harbor, Washington. U.S. Army Corps of Engineers, Seattle District., 16 p.

Phipps, J. B., Hemphill-Haley, E., & Atwater, B. F. (2015). Chance findings about early Holocene tidal marshes of Grays Harbor, Washington, in relation to rapidly rising seas and great subduction earthquakes: U.S. Geological Survey Scientific Investigations Report 2015-5063, P. 36. http://dx.doi.org/10.3133/sir20155063. Accessed January 10, 2016. https://doi.org/10.3133/sir20155063

Robinson, S. W., & Thompshon, G. (1981). Radiocarbon corrections for marine shell dates with application to southern Pacific Northwest Coast prehistory. *Syesis, 14*, 45-57.

Ruggiero, P., Kaminsky, G. W., Komar, P. D., & McDougal, W. G. (1997). Extreme waves and coastal erosion in the Pacific Northwest. In Proceedings of Waves '97 ASCE pp. 947-961.

Satake, K., Shimazaki, K., Tsuji, Y., & Ueda, K. (1996). Time and size of giant earthquake in Cascadia inferred from Japanese tsunami records of January 1700. Nature, 378, 246-249. https://doi.org/10.1038/379246a0

Scheidegger, K. F., & Phipps, J. B. (1976). Dispersal patterns of sands in Grays Harbor, estuary, Washington. *Journal of Sedimentary Petrology, 46*, 163-166.

Smith, D. G. (1988). Modern point bar deposits analogous to the Athabasca oil sands, Alberta, Canada. *Tide influenced sedimentary environments and facies: D. Reidel Publishing Company*, 417-432. https://doi.org/10.1007/978-94-015-7762-5_27

Stuiver, M., Reimer, P. J., & Reimer, R.W. (2017). CALIB 7.1. Retrieved December 12, 2017, from http://calib.org

Twichell, D. C., Cross, V., & Peterson, C. D. (2010). Partitioning of sediment on the shelf offshore of the Columbia River littoral cell. *Marine Geology, 273*, 11-31. https://doi.org/10.1016/j.margeo.2010.02.001

USACE. (1903). Improvement of certain rivers and harbors in Washington. Annual Report To The Chief Engineers, Office Of The Chief Engineer, United States Army, Washington, pp. 620-625.

USACE. (2017). Corps of Engineers report for annual maintenance dredging in Grays Harbor (year 2017). http://www.nws.usace.army.mil/Media/News-Releases/Article/1113828/corps-of-engineers-to-start-grays-harbor-outer-harbor-maintenance-dredging-apri/. Accessed online line December 18, 2017.

USCGS. (1973). United States Coast and Geodetic Survey Bathymetric Chart 6195, Grays Harbor, Washington. Department of Commerce, Washington DC

USGS. (20173b). RunWaveCalcs.html, Linear wave calculations for bottom orbital velocities. US Geological Survey Applet. Retrieved December 1, 2017, from http://woodshole.er.usgs.gov/staffpages/csherwood/sedx_equations/RunWaveCalcs.html

USGS. (2017a). SPMWave.html, Fetch and depth limited wave calculations. US Geological Survey Applet. Retrieved December 1, 2017, from http://woodshole.er.usgs.gov/staffpages/csherwood/sedx_equations/RunSPMWave.html

Vanderburgh, S., Roberts, M. C., Peterson, C. D., Phipps, J. B., & Herb, A. (2010). Holocene transgressive and regressive deposits of the Columbia River littoral cell barriers and beach plains., *Marine Geology, 273*, 32-43. https://doi.org/10.1016/j.margeo.2010.02.002

WSDA. (2016). Progress of the 2016 *Spartina* Eradication Program. Washington State Department of Agriculture~2016 Progress Report. p. 31. Retrieved February 25, 2018, from https://agr.wa.gov/FP/Pubs/docs/pp/505-SpartinaReportFinal2016.pdf

WWW Tide. (2018). WWW Tide/Current Predictor: Biological Sciences, University of South Carolina. Retrieved November 11, 2017, from http://tbone.biol.sc.edu/tide

Zaitlin, B. A., Dalrymple, R. W., & Boyd, R. (1994). The stratigraphic organization of incised–valley systems associated with relative sea–level change. SEPM Society for Sedimentary Geology, special Publication No. 51, 45-60.